Organic Geochemistry 185 (2023) 104674

Contents lists available at ScienceDirect

Organic Geochemistry

journal homepage: www.elsevier.com/locate/orggeochem

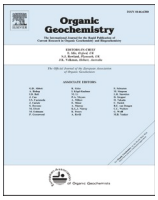

Hydrogen isotope biogeochemistry of plant waxes in paired lake catchments

Mariliis Eensalu [a,b,*], Daniel B. Nelson [c], Anna Buczynska [a], Oliver Rach [d], Eric S. Klein [e], Justin P. Dodd [a], Anneli Poska [b], Nathan D. Stansell [a]

[a] Department of Earth, Atmosphere and Environment, Northern Illinois University, Dekalb, IL 60115, USA
[b] Department of Geology, Tallinn University of Technology, Tallinn 19086, Estonia
[c] Department of Environmental Sciences – Botany, University of Basel, Basel 4056, Switzerland
[d] Helmholtz Centre Potsdam – GFZ German Research Centre for Geosciences, Organic Surface Geochemistry Lab, Section 4.6: Geomorphology, Potsdam 14473, Germany
[e] Department of Geological Sciences, University of Alaska Anchorage, Anchorage, AK 99508, USA

ARTICLE INFO

Associate Editor–**Josef P. Werne**

Keywords:
Deciduous plants
Estonia
Isotope fractionation
Leaf water
Leaf wax
n-Alkane
Terrestrial biomarker

ABSTRACT

Studies of plants in modern catchment systems can serve to improve the level of understanding of sedimentary plant wax hydrogen isotope (δ^2H) data by directly investigating the link between local climate conditions, plant source water, leaf water, and plant lipids for individual plant species. Here we present such an application to compare two lake catchments with different basin morphologies in Estonia. We sampled leaf and xylem water, as well as leaf waxes from the seven common plant species in each catchment, and soil water. We then measured the δ^2H values of all waters, and of *n*-alkanes (δ^2H_{n-alk}) from the plant waxes, as well as surface lake sediments. We applied a Péclet modified Craig-Gordon leaf water model using local precipitation isotope and climate data to characterize the δ^2H values of the biosynthetic source water pool throughout the entire growth season. The data and model results provide a detailed view of how the input hydro-climatic signals from the precipitation δ^2H values were modified by environmental and plant physiological conditions and ultimately by the biosynthetic isotope fractionation associated with *n*–alkane production by each plant species. We report both average apparent ($\varepsilon_{app} = -92 \pm 21$ ‰) and biosynthetic ($\varepsilon_{bio} = -132 \pm 19$ ‰) hydrogen isotope fractionation factors of all species from the studied catchments. This information serves as a foundation for sedimentary organic geochemistry and paleoclimate studies, which allows for more direct and quantitative links to be made between sedimentary plant wax δ^2H values and the climate signal contained in plant source water.

1. Introduction

Lake sedimentary archives contain information about past trends in hydroclimate. In particular, the hydrogen isotopic composition of leaf wax *n*-alkanes (δ^2H_{n-alk}) extracted from sediments are widely used to reconstruct the hydrogen isotopic composition of past environmental waters (Sachse et al., 2004; Shuman et al., 2006; Rach et al., 2014). However, biomarker profiles are catchment specific as the surrounding vegetation differs spatially and temporally, which requires careful characterization when utilizing δ^2H_{n-alk} for modern and paleo-studies. There are a series of hydrogen isotopic fractionation stages between the source water of a plant, which is commonly assumed to be local precipitation (δ^2H_{precip}), and the leaf wax *n*-alkanes that are ultimately produced by plants during growing seasons. These multiple isotope fractionations can be grouped to describe the single most directly relevant and easily measured net effect between precipitation and lipids, or apparent fractionation (ε_{app}). Previous work has demonstrated that this varies greatly among species, latitudes and environments (Smith and Freeman, 2006; Feakins and Sessions, 2010; Sachse et al., 2012; Berke et al., 2019). For example, the δ^2H_{precip} signal in an ecosystem can be transformed from its original value by site-specific evaporation from soils, transpiration in the plant leaf, and finally through biosynthesis (ε_{bio}) of *n*-alkanes (Smith and Freeman, 2006; McInerney et al., 2011). Evapotranspiration causes differences in plant source water, and variability in the water pools is also affected by plant rooting depth and plant taxonomy (Freimuth et al., 2019). Moreover, although there is a strong relationship between annual precipitation δ^2H_{precip} and soil water δ^2H (δ^2H_{sw}) values, it is likely that the plants in high mid–latitude

* Corresponding author at: Department of Earth, Atmosphere and Environment, Northern Illinois University, Dekalb, IL 60115, USA.
E-mail address: meensalu@niu.edu (M. Eensalu).

https://doi.org/10.1016/j.orggeochem.2023.104674
Received 15 June 2023; Received in revised form 7 September 2023; Accepted 7 September 2023
Available online 9 September 2023

regions record a δ^2H_{precip} signal that is time integrated in the soil over weeks to months leading up to the timing of leaf flush, when most plant waxes are formed (Sachse et al., 2010; Tipple et al., 2013; Brinkmann et al., 2018). As such, reconstructing past δ^2H_{precip} from sedimentary biomarkers without information about local plant fractionation factors could result in a significant bias. Also, deciduous trees tend to produce more *n*-alkanes compared to other plants (Sachse et al., 2006) and thus δ^2H_{n-alk} signals in temperate regions are skewed towards trees and shrubs (Freimuth et al., 2019). Therefore, detailed surveying of the local hydrogen isotope ecohydrology in modern biomes can greatly improve modern and paleo-applications that seek to utilize δ^2H_{n-alk} values from sediments.

Understanding how modern climate conditions (relative humidity and temperature) affect δ^2H fractionation in plants allows for characterizing the ecohydrological shifts in response to changing climate parameters. This relationship can then be applied to paleo-archives which contain the same δ^2H_{n-alk} biomarkers that formed in the past to estimate the timing and magnitude of hydrological changes in a catchment area (Rach et al., 2017). Furthermore, combining the paleo δ^2H_{precip} values with additional proxies such as $\delta^{18}O$ values from the same lake basin would provide information on past air mass trajectories, such as the second order parameter deuterium excess ($\delta^2H - 8 \times \delta^{18}O$), information which is limited with using $\delta^{18}O$ data alone (Jouzel and Merlivat, 1984; Klein et al., 2016).

The δ^2H_{n-alk} records collected at a catchment level offer a potentially unique and valuable perspective of past climate changes. To date, several studies have focused on defining ε_{app} for species in the northern mid and high latitudes (Sachse et al., 2004; Smith and Freeman, 2006; Kahmen et al., 2013a; Berke et al., 2019; O'Connor et al., 2020) with only a few scattered records in Scandinavia (Sachse et al., 2006; Yang et al., 2011; Balascio et al., 2018a) and central Europe (van den Bos et al., 2018). These studies, however, focus on local plant species from which the biome in Estonia differs considerably. There are currently also no detailed studies from the eastern and northern Baltic region, hindering our comprehensive understanding of current and past environmental changes in northern Europe based on sedimentary δ^2H_{n-alk} records.

Reconstructing quantitative relative humidity change on a local level (Rach et al., 2017) calls for knowledge of the past local vegetation composition. Lake sediments contain a mixture of plant waxes that formed in the surrounding ecosystem, and the relative abundance of species in the catchment area influences the response to changes in climate recorded in the sediment (Sachse et al., 2012; Diefendorf and Freimuth, 2017). Furthermore, leaf water ^2H enrichment due to transpiration makes up a major component of ε_{app} values. The magnitude of this effect is itself a function of not only the source water δ^2H values, but also environmental factors, with the main drivers being temperature and relative humidity (Cernusak et al., 2016). Changes in these drivers constitute climatic changes on their own, and can thereby reduce the level of independence with which climatic inferences can be made based on sedimentary δ^2H_{n-alk} values alone. In this regard, δ^2H_{n-alk} values from terrestrial plants may be more directly considered as a proxy for leaf water δ^2H values, with the difference between leaf water and plant source water δ^2H values being largely controlled by temperature and relative humidity. There is, nevertheless, a strong correlation between δ^2H_{n-alk} values and mean annual precipitation δ^2H values (Ladd et al., 2021), but this relationship does contain considerable variability at regional scales, and components of this pattern may not be stable within a given region over time.

In cases where modern leaf water δ^2H values can be characterized, the δ^2H values of leaf water can be used with δ^2H_{n-alk} values to calculate biosynthetic isotope fractionation (ε_{bio} values). Although studies have shown that these too may vary, these changes are more generally driven by seasonal changes that may not affect the major hydrogen isotope signal that is exported from plant to sediment (Newberry et al., 2015), or by extreme conditions that may not be likely in nature (Cormier et al., 2018; Baan et al., 2023). ε_{bio} values can also be expected to be more stable over time than ε_{app} values, and may thus provide a more unbiased tool for quantitative conversion of δ^2H_{n-alk} values into a climatically relevant water δ^2H value. Unfortunately, due to the comparative difficulty in determining ε_{bio} values, fewer studies have done so as compared to ε_{app} values.

The paired observation of leaf waters and waxes allows for characterization of the local ε_{bio} and ε_{app} values. Here we studied the δ^2H of water and leaf waxes from seven common angiosperm species in Estonia, and modeled their leaf water δ^2H based on environmental data at two sites with different hydrologic properties (Fig. 1), the open-basin Lake Nuudsaku (58°11′24″ N, 25°37′32″ E) and the semi-closed-basin Lake Pangodi (58°11′24″ N, 26°34′29″ E). We set up this study to test if (1) similar vegetation in the same general region would record the same environmental signal at the two lakes with different basin morphology, and (2) whether the ε_{bio} and ε_{app} determined in these ecosystems would, with the aid of leaf water modeling, agree with such values from other high mid-latitude sites. We documented the range of variability in the plant-level fractionation factors and observed how each of these specific ecosystems transfer the δ^2H signal from the hydroclimate to modern plants and to lake sediments. We draw conclusions based on the applicability of these data in the studied catchments with implications for reconstructing past hydroclimate dynamics.

2. Study site

2.1. Lake catchments

Lakes Nuudsaku (58°11′49″ N, 25°37′39″ E) and Pangodi (58°11′45″ N, 26°34′40″ E) are located in southern Estonia (Fig. 1). Lake Nuudsaku is a small lake with a surface area of 8 ha and a catchment area of 6.2 km^2; Lake Pangodi surface area is remarkably larger, 93.3 ha, with a similar catchment area of 7.6 km^2 (Keskkonnaagentuur, 2022). They are both underlain by Devonian sandstones capped with Quaternary deposits associated with Scandinavian glaciation (Kalm, 2006). With a maximum water depth of ~ 4.6 m, Lake Nuudsaku is surficially open with a seasonally active overflow and is fed by active springs and near-surface groundwater. Pangodi has a maximum water depth of ~ 9.0 m, negligible inflows and outflows, and a large surface area to volume ratio that makes it sensitive to summer evaporation. Stansell et al (2017) reported warm season (May to October) lake water isotope $\delta^{18}O$ values of –10.1 ± 0.5 ‰ from Nuudsaku (n = 14) and –6.6 ± 0.9 ‰ from Pangodi (n = 4), and δ^2H values of –73.4 ± 3.0 ‰ from Nuudsaku and –54.1 ± 6.2 ‰ from Pangodi. Based on field titrations of Lakes Nuudsaku and Pangodi in August of 2014, the alkalinity values of the lake waters were 211 mg/l and 154 mg/l, respectively. Both lakes preserve laminated to banded sediment layers with little evidence of bioturbation and wind mixing. Dissolved oxygen values for Lake Pangodi ranged from 10.1 mg/l in the epilimnion to 4.7 mg/l in the hypolimnion in August of 2014, and the lake is slightly oligotrophic based on the classification scheme of Carlson (1977). Dissolved oxygen values for Lake Nuudsaku range from 7.1 mg/l in the epilimnion to 0.4 mg/l in the hypolimnion, and the lake is slightly eutrophic. Local forests are best described as (Euro-Siberian) boreal mixed coniferous and temperate deciduous forests. The Corine land cover map characterizes the local vegetation at Pangodi as land principally occupied by agriculture (with significant areas of natural vegetation), mixed forest and natural grassland. A recent study on Lake Pangodi pollen shows that the surface sediment profile consists of 25 % broad and 22 % needle leaved trees, 2 % of shrub, 34 % of herb and 18 % of grass vegetation (Palusalu et al., 2023). Lake Nuudsaku is also mostly surrounded by agricultural land, mixed forest, pastures and coniferous forests (https://land.copernicus.eu/pan-european/corine-land-cover/clc2018).

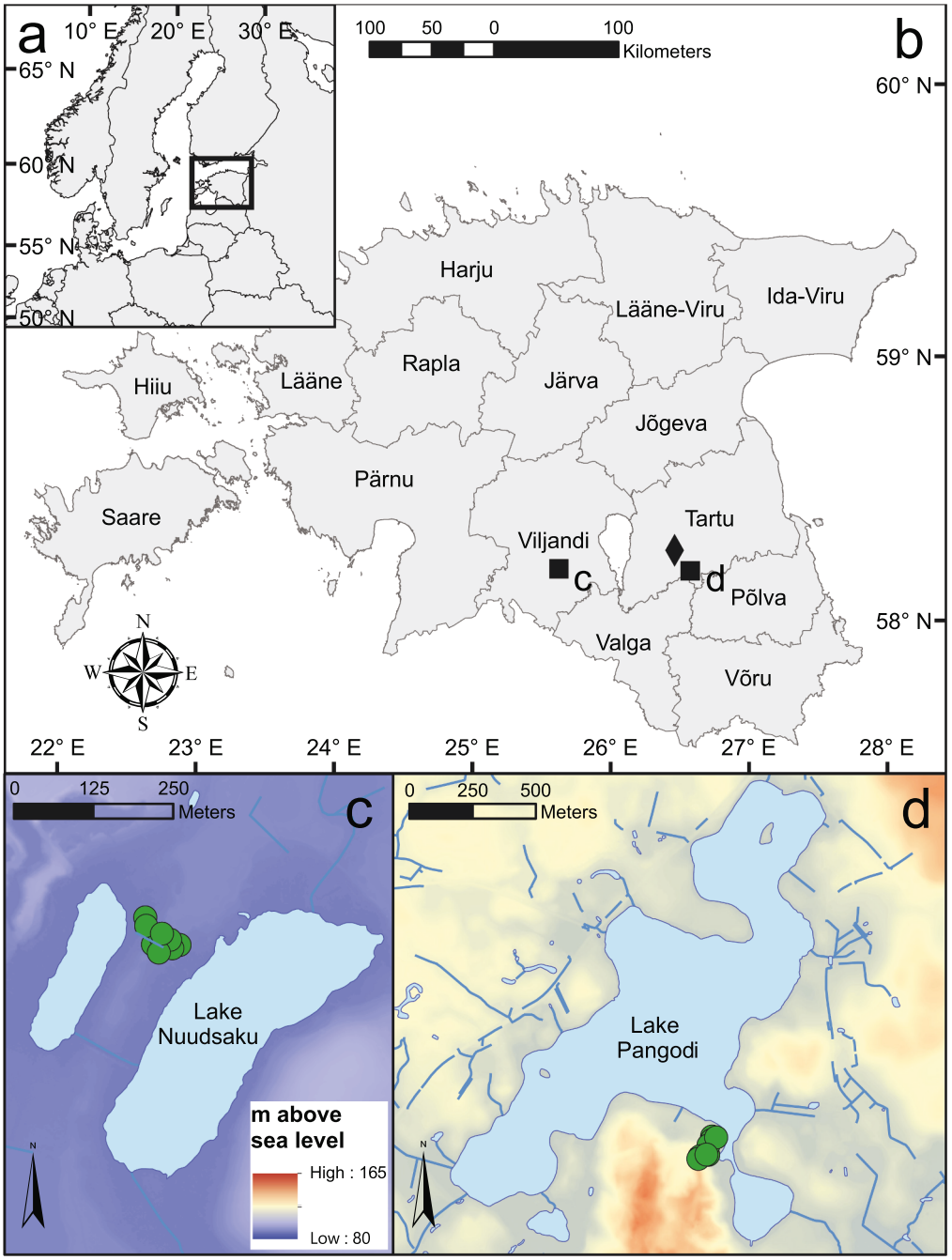

Fig. 1. Map of the study locations in northern Europe. The first panel shows Europe (a) with the box drawn around Estonia. Map of Estonian counties (b) with Tartu-Tõravere meteorological station is shown as a diamond, and the open-basin Lake Nuudsaku (c) and semi-closed-basin Lake Pangodi (d) as black squares. Green circles in panels c and d represent soil and plant sampling locations. Elevation legend (meters above sea level) shown on a digital terrain model (1 m resolution) by Estonian Land Board (LAZ 1.4 LiDAR data from 2017 to 2021) applies to both bottom panels. (For interpretation of the references to colour in this figure legend, the reader is referred to the web version of this article.)

2.2. Climate and water isotopes

Climate conditions at Nuudsaku and Pangodi are relatively similar (Fig. 2). The annual precipitation in Estonia ranges from 500 to 700 mm while about 80% of that is lost to evaporation; the mean cold and warm season temperatures are usually –1 °C and 13 °C, respectively (Estonian Meteorological Survey, https://www.ilmateenistus.ee/kliima/ajalool ised-ilmaandmed/). Based on Estonian Meteorological Survey data from 2004 to 2021 (data acquired from the same link as above), the mean annual temperature is 8.9 °C in Tartu-Tõravere (Pangodi) and 6.5 °C in Viljandi (Nuudsaku).

The Global Networks of Isotopes in Precipitation measurements at Tartu-Tõravere station (location shown in Fig. 1) from 2013 to 2018 show that the modern $\delta^{18}O$ values of precipitation ($\delta^{18}O_{precip}$) ranged from –15.1 ‰ (vs VSMOW) in February to –7.7 ‰ in June with an average (mean) yearly value of ~ –11 ‰ (Fig. 2). Similarly, the $\delta^{2}H_{precip}$ values varied from –114 ‰ (vs VSMOW) in February to –54 ‰ in June with the yearly values averaging at –80 ‰ (1 standard deviation (1σ) = 24). Deuterium excess values (d-excess, defined as $\delta^{2}H - 8 \times \delta^{18}O$) were lowest in May (5.4 ‰) and highest in November (10.8 ‰) with an annual average of ~ 8.1 ‰, based on the measurements (https://www.iaea.org/water). These measured values are consistent with the range of

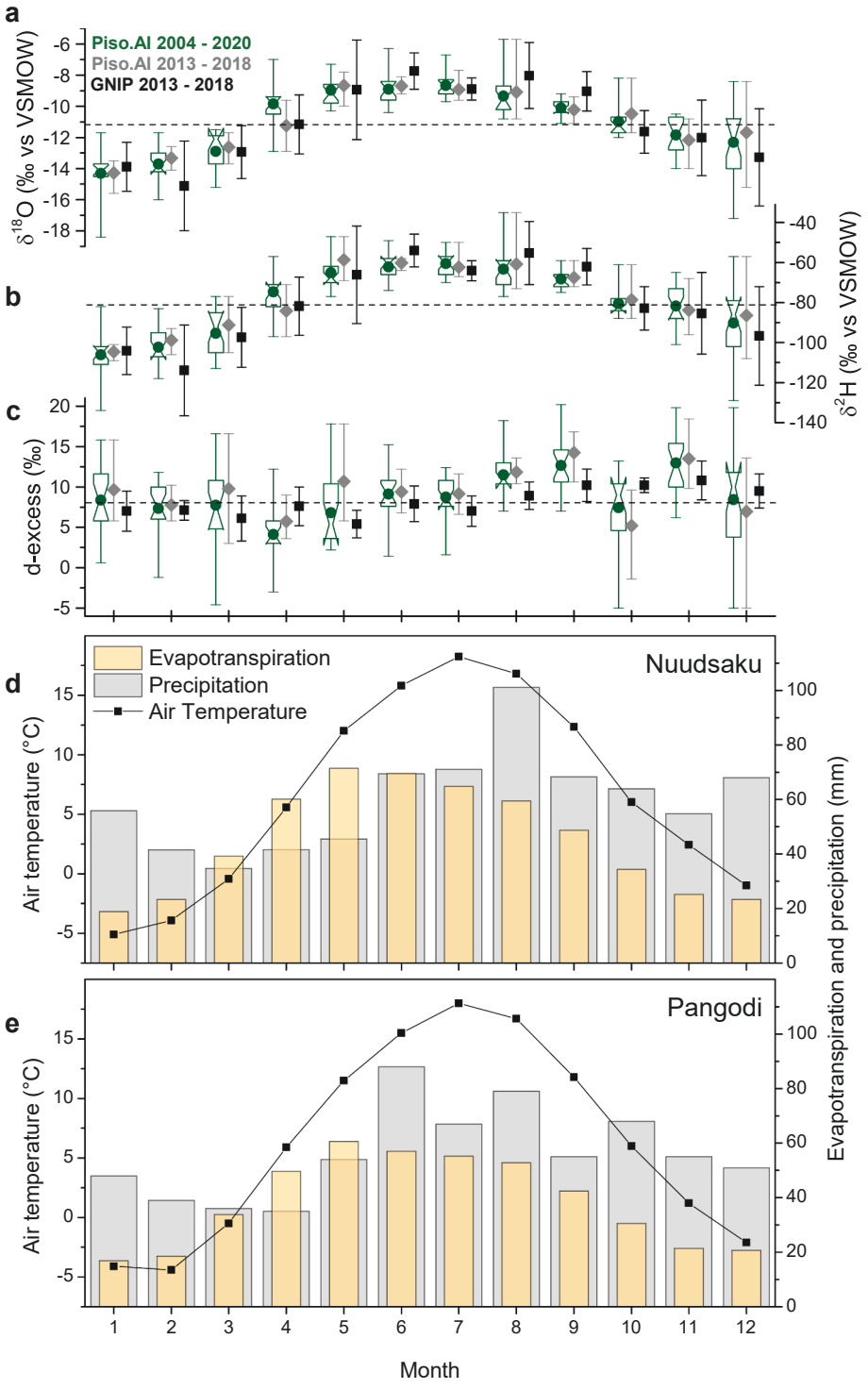

Fig. 2. Monthly averages of precipitation $\delta^{18}O$ (a), $\delta^{2}H$ (b) and d-excess (c) with error bars at Tartu-Tõravere Global Network of Isotopes in Precipitation (GNIP) station (58° 15′ 51″ N, 26° 27′ 41″ E) from 2013 to 2018 (IAEA, 2022) as black boxes. Gray and notched green boxes represent modeled Piso.AI data from 2013 to 2018 and from 2004 to 2020, respectively (Nelson et al., 2021). The yearly averages are represented by gray horizontal lines. Two bottom plots represent monthly averages of precipitation, temperature (2004–2020; http://www.ilmateenistus.ee/kliima/) at Viljandi (Nuudsaku) and Tartu-Tõravere (Pangodi), and modeled evapotranspiration (using R package Evapotranspiration) at Nuudsaku (d) and Pangodi (e) based on 2011 – 2020 climatological data at Tartu-Tõravere station. (For interpretation of the references to colour in this figure legend, the reader is referred to the web version of this article.)

modeled precipitation isotope values over longer timescales from Piso.AI (Nelson et al., 2021).

3. Materials and methods

3.1. Field sampling of leaves, xylem, soil, lake water and surface lake sediment

A total of seven plant species were selected for sampling based on their occurrence in the lake catchment areas. A site was defined as an area with a maximum radius of 100 m in diameter, and one site was sampled at either catchment. The species selected for the study at each of our study sites were representative of the entire vegetation surrounding the lakes. Angiosperms tend to produce more *n*–alkanes than gymnosperms, and for this reason, the angiosperms were selected for the study in particular as the leaf wax signal of these species is reported to make up the majority of sedimentary *n*-alkanes (Sachse et al., 2006; Freimuth et al., 2019). *Acer platanoides* (Norway maple), *Corylus avellana* (common hazel), *Quercus robur* (English oak) and *Sorbus aucuparia* (rowan) were sampled at both locations with the addition of *Vaccinium myrtillus* (European blueberry) and *Alnus incana* (grey alder) in the Pangodi catchment, and *Alnus glutinosa* (black alder) in the Nuudsaku catchment. Two individual trees/shrubs were selected per species at each location and sampled in duplicate for xylem water, leaf water, and leaf wax hydrogen isotope analyses. Field work was conducted on days with no precipitation, June 20th and July 7th, 2021. Leaves, branches and roots were sampled between 10 am and 4 pm, soil water between 9 am and 6 pm on the same field days.

Larger petioles were removed from each mature whole leaf and the remaining leaves placed in 12 ml airtight 738 W (Labco) exetainers. For xylem extraction, non-green tree twigs were cut 40 – 60 cm basipetal to the sampled leaves for preventing contamination by enriched leaf waters. Root crowns of *Vaccinium myrtillus* were sampled at least 3 cm below the soil surface and any green components were removed (Barnard et al., 2006). Sharp knives were used to remove phloem tissue from the outer layers of the branches and roots, and the remaining xylem was stored in exetainers.

Soil cores were obtained for soil water hydrogen isotope analyses at multiple depths in both catchments in the vicinity of the sampled vegetation. A 70 cm stainless steel soil corer with a 2 cm diameter was used to collect soil, from which to extract soil water with a purpose of assessing the approximate depths from which the sampled plants draw their water, and to examine the isotopic variation in the soil column. Sub-samples at 10 – 14 and 40 – 44 cm depths were collected from the soil core in the same type of Labco exetainer as was used for xylem and leaf water samples (marked as samples from 10 and 40 cm, respectively). Duplicate soil cores were acquired at lower and higher elevations at both sampling sites. Each sample acquisition time was recorded. All leaf, xylem and soil samples were immediately sealed in the field and placed in an insulated thermal field bag equipped with two large cooling elements. At the end of each sampling round, the filled vials were sealed with parafilm, transferred to lab-grade cold boxes for transport and kept frozen until laboratory procedures. The uppermost 20 cm of sediment from the center of both lakes were collected using a piston corer with polycarbonate tubing attached. The sediments were extruded in the field at 0.25 cm intervals and stored in sealed plastic bags.

3.2. Environmental data loggers

A TFA Dostmann 31.1054 LOG32TH hygro-thermometer was installed ~ 2 m above ground level at the Nuudsaku sampling location on June 5th, 2021. The automated logger continuously recorded temperature (–40 to 70 °C; resolution 0.1 °C), dewpoint and relative humidity (RH, 0 to 100 %, resolution 0.1 % RH) at 10-minute intervals. For the Pangodi location, these data were acquired from the Estonian Meteorological Survey (Tartu-Tõravere station, location shown on Fig. 1). The Nuudsaku logger data was interpolated to hourly intervals using the FORECAST function in Excel. The logger data was then compared to the national weather station climate logs in Viljandi using a two-sample T–test for variance to check if the local self-installed temperature and RH were corresponding to the regional observations. At the 0.05 level, the populations were not significantly different. Since there is no local data available for Pangodi, we use national weather station climatological data as an input to the isotope models (discussed below) for both catchments in our study.

3.3. Water extraction and stable isotope analysis

Water from xylem (n = 84), leaf (n = 84) and soil (n = 36) samples was extracted using a cryogenic vacuum line at University of Basel as described by Newberry et al. (2017). Twenty samples were processed at a time, the extracted water volume measured using a single-use syringe and the plant water transferred into a 1.5 ml vial for instrumental analysis. Extracted water δ^2H and $\delta^{18}O$ values were analyzed using a Thermal Conversion / Elemental Analyzer (TC/EA) coupled to a Delta V Plus isotope ratio mass spectrometer (IRMS) through a ConFlo IV interface (Thermo Fisher Scientific, Bremen, Germany). Each sample was injected at least six times to overcome memory effects from preceding samples, and the retained measured values were pooled and normalized to the VSMOW/SLAP scale using calibrated lab standards with δ^2H values of –76.4 ‰ and 45.1 ‰, and $\delta^{18}O$ values of –10.7 ‰ and 4.3 ‰, respectively. Lab analytical precision, calculated as one standard deviation of repeat analyses of a quality control sample, was 0.4 ‰ for δ^2H measurements (n = 370), and 0.12 ‰ for $\delta^{18}O$ measurements (n = 370) in 2021, the year in which all water measurements for this study were made.

The measured xylem water δ^2H values ($\delta^2H_{xyl-meas}$) were corrected for cryogenic extraction effects to calculate the corrected xylem water δ^2H ($\delta^2H_{xyl-corr}$) following Chen et al. (2020):

$$\delta^2H_{xyl-corr} = \left(\frac{\delta^2H_{xyl-meas} + 1}{\varepsilon_{cryo-corr} + 1}\right) - 1 \quad (1)$$

where $\varepsilon_{cryo-corr}$ denotes the estimated offset of –8.1 ‰ between the $\delta^2H_{xyl-meas}$ and the $\delta^2H_{xyl-corr}$.

Evaporative isotope effects were calculated for water samples as the line-conditioned (LC) excess (Landwehr and Coplen, 2006) in equation (2):

$$LC-excess = \delta^2H_{sample} - LMWL_{slope} \times \delta^{18}O_{sample} - LMWL_{intercept} \quad (2)$$

where δ^2H_{sample} and $\delta^{18}O_{sample}$ represent xylem water samples in respect to the LMWL.

3.4. Lipid extraction and biomarker quantification

A total of 42 dry plant leaf samples were placed in Erlenmeyer flasks. The samples were spiked with 25 µl of 0.15 mg/l 5-α-androstane. Samples in capped flasks were placed in a Fisher Scientific FS30 Ultrasonic bath three times for 20 min using 30 ml of 9:1 v/v dichloromethane/methanol (DCM/MeOH). The solvent containing total lipid extract (TLE) was pipetted out after every sonication round. The *n*–alkane aliphatic fraction was separated from the TLE by eluting the samples with 12 ml of hexane through glass syringes with activated silica gel (VWR high purity irregular, 40 – 60 µm, 60 Å) equipped with 13 mm GF/A (Whatman) filters in the bottom, mounted on a Solid Phase Extraction block (Supelco Visiprep™). Sulphur was removed using activated copper (<425 µm Aldrich) columns, and *n*-hexane was used as eluent (6 ml). Samples were concentrated under N–EVAP™111 nitrogen evaporator (Organomation Associates, Inc.) and stored in airtight 1.5 ml amber vials. Surface lake sediment samples were processed using the same method. Unsaturated compounds from the aliphatic sediment sample fractions were removed by eluting the samples with 6 ml of

hexane through activated $AgNO_3$ coated silica gel (+230 mesh) columns.

The leaf *n*-alkanes were identified and quantified using a gas chromatograph attached to a mass spectrometer (GC–MS–QP2010S, Shimadzu Scientific Instruments, Kyoto, Japan) at Northern Illinois University. An *n*-C_7–C_{40} alkane standard (1000 μg/ml each component in hexane, Supelco, Sigma Aldrich, MO, USA) together with 5–α–androstane (Sigma Aldrich, MO, USA) as an internal standard were used for quantitation. Compounds were separated on a DB5–MS column (Agilent Technologies, 30 m length, 0.25 mm i.d., and 0.25 μm film thickness) with a splitless injection at 290 °C. The GC temperature was kept at 60 °C for 1 min, followed by a temperature gradient of 10 °C/min to 170 °C and afterwards, of 4 °C/min to 300 °C. Ten samples were run in duplicates. Relative standard deviation (RSD) was generally below 14 % for all analytes, exceeding that value in <15 % of cases. The average RSD was 8 %. Percent error between expected and calculated amounts for a quality control standard containing *n*–C_{27}, *n*–C_{31} and *n*–C_{33} alkanes at three different concentration levels, was below 21 % (injections at the beginning, in the middle and at the end of the measurement sequence).

3.5. Stable hydrogen isotope analysis of n-alkanes

Hydrogen stable isotopes were measured using the GC-HTC-IRMS system (Trace GC Ultra interfaced to a MAT253, Thermo Scientific, Bremen, Germany). Compounds were separated on a DB5-MS column (Agilent Technologies, 30 m length, 0.25 mm i.d., and 0.25 μm film thickness). A 2–minute spitless injection was used at 280 °C. The GC temperature was kept at 70 °C for 3 min, followed by a temperature gradient of 10 °C/min to 150 °C and afterwards, by a gradient of 4 °C/min to 320 °C. The high temperature conversion oven was kept at 1420 °C. δ^2H values were normalized to the VSMOW scale using a mixture of *n*-alkanes obtained from Indiana University. Stable hydrogen isotope ratios of these standards were measured off-line according to Schimmelmann et al. (1999) at Indiana University. H_3^+ factor was measured before every major sequence run, which was between 4 and 5 ppm nA^{-1} during the period of a few months when these samples were analyzed. When measured daily, 1σ values of 0.03 were obtained for two consecutive daily measurements. All samples were injected at least twice. Additional *n*-alkane standard was used to monitor the precision of these measurements. The δ^2H value of *n*-C_{30} alkane peak was –45.3 ± 3.4 ‰ for 12 injections on different days (one outlier with a lower peak area was excluded). Surface lake sediment samples from Lake Nuudsaku and Lake Pangodi each were processed and analyzed for δ^2H_{n-alk} values at Basel University, Switzerland following the methods applied to aerosol samples as described in Nelson et al. (2018). All results are reported with respect to Vienna Standard Mean Ocean Water (VSMOW) in per mil (‰) notation. Surface lake sediment *n*-alkane relative distributions were calculated by normalizing the δ^2H_{n-alk} peak area to the most abundant compound.

3.6. Data analysis and machine learning model

The isotopic fractionation factors ($\varepsilon_{a/b}$) between two substances (either measured or modeled) were calculated using the formula (Coplen, 2011)

$$\varepsilon_{a/b} = \alpha_{a/b} - 1 = \left(\frac{\delta^2H_a + 1}{\delta^2H_b + 1}\right) - 1 \quad (3)$$

For example, ε_{app} (apparent isotopic fractionation) was calculated using formula (3) between source water δ^2H (δ^2H_{LMWL}; δ^2H_b in equation (3)) and δ^2H_{n-alk} (δ^2H_a in equation (3)). The same formula was used to estimate leaf water δ^2H (δ^2H_{lw}; δ^2H_a in equation (3)) ^{2}H-enrichment above $\delta^2H_{xyl-corr}$ (δ^2H_b in equation (3); $\varepsilon_{l/x}$), apparent and biosynthetic fractionation (ε_{bio}).

Carbon preference index (CPI) characterizes the relative abundance of odd over even chain length *n*-alkane (Bray and Evans, 1961; Herrera-Herrera et al., 2020) and was calculated using the following formula:

$$CPI = \frac{1}{2} \times \left(\frac{\sum C_{25-33}^{odd}}{\sum C_{24-32}^{even}} + \frac{\sum C_{25-33}^{odd}}{\sum C_{26-34}^{even}}\right) \quad (4)$$

Average carbon chain length (ACL) was calculated using an equation by Maffei (1996):

$$ACL = \frac{\sum C_i \times i}{\sum C_i} \quad (5)$$

where C_i stands for the relative amount of the *n*-alkanes (*n*-C_{23} – *n*-C_{35}) with a specific number of *i* carbons.

We also applied a machine learning model Piso.AI which is trained on geographic and climate data to predict monthly time series of oxygen and hydrogen isotope values of precipitation with prediction errors of 1.7 ‰ for $\delta^{18}O$ values and 13 ‰ for δ^2H values (Nelson et al., 2021). The Piso.AI modeled yearly average δ^2H_{precip} from 2013 to 2018 was –78 ‰ which is in an agreement with the observational data. We then ran the Piso.AI model for a longer period spanning between 2004 and 2020 as we used meteorological data from that time frame to model the local precipitation and evapotranspiration at both catchments (Fig. 2). This model run resulted in an average annual δ^2H_{precip} value of –79 ‰.

3.7. Leaf water δ^2H modeling

Leaf water δ^2H values were modeled from meteorological data in order to characterize variability in the biosynthetic source water pool for *n*-alkane production over the whole growing season. Modeled values were checked for accuracy against the measured values from the summer of 2021. The $\delta^2H_{xyl-corr}$ value along with the corresponding individual δ^2H_{lw} values were used to calculate the isotopic enrichment at the evaporative site in the leaves (Δ_e) by applying the Craig-Gordon evaporation model (Cernusak et al., 2016; Craig and Gordon, 1965; Farquhar et al., 2007):

$$\Delta_e = (1+\varepsilon^+)\left[(1+\varepsilon_k)\left(1-\frac{e_a}{e_i}\right) + \frac{e_a}{e_i}(1+\Delta_V)\right] - 1 \quad (6)$$

where the actual vapor pressure (e_a) was calculated from saturation vapor pressure (SVP). The SVP was calculated from temperature and pressure and the measured RH, after Buck (1981). Vapor pressure deficit (VPD) is defined as VPD = SVP – e_a. Leaf internal vapor pressure (e_i) was calculated after Clifton-Brown and Jones (1999). Equilibrium fractionation (ε^+) and kinetic fractionation (ε_k) were calculated following Cernusak et al. (2016). Stomatal conductance was estimated from VPD after West et al. (2008).

The Δ_V is the enrichment of atmospheric water vapor relative to source water, which we assume it to be in equilibrium with:

$$\Delta_V = \varepsilon^+ \quad (7)$$

As the evaporated leaf water mixes with the constant inflow of xylem water to the leaf, the Craig-Gordon model alone overestimates the whole-leaf ^{2}H-enrichment in leaf water. Therefore, we applied a Péclet correction ($\wp$) that describes the ratio between transpiration and diffusion:

$$\wp = \frac{L \times E}{C \times D_H} \quad (8)$$

where C is the molar concentration of water (5.55×10^4 mol/m^3). The ^{2}H diffusivity in water (D_H) was calculated following Cernusak et al. (2016). Effective path length (L) of water moving through the plant mesophyll was calculated after Song et al. (2013); E is the transpiration rate which was calculated from

$$E = \frac{\left(\frac{e_i}{10} - \frac{e_a}{10}\right)}{100} \times \left(\frac{1}{r_b + r_s} \times 1000\right) \quad (9)$$

where the r_s is the stomatal and r_b is the boundary layer resistance (m^2 s/mol). This calculation resulted in a different Péclet correction value for all sampled individuals (n = 42) which ranged between 0.1456 and 0.1773 (June mean value 0.1508, 1σ = 0.0046; July mean value 0.1707, 1σ = 0.0036).

The Péclet number was applied to calculate the leaf water enrichment (Δ_L) (Farquhar and Lloyd, 1993):

$$\Delta_L = \Delta_e \left(\frac{1 - e^{-\wp}}{\wp}\right) \quad (10)$$

The leaf water δ^2H value was then modeled ($\delta^2H_{lw\text{-}mod}$) at the time of field sampling:

$$\delta^2 H_{lw-mod} = \left(\Delta_L + \delta^2 H_{xyl-corr}\right) + \frac{\left(\Delta_L \times \delta^2 H_{xyl-corr}\right)}{1000} \quad (11)$$

The $\delta^2H_{lw\text{-}mod}$ values from each species from different locations and sampling dates were then compared to the measured δ^2H_{lw} values by correlation analysis ($p \leq 0.05$). All correlation coefficients presented in this study are statistically significant ($p \leq 0.05$), unless stated otherwise.

3.8. Modeled mean leaf water δ^2H during leaf formation and isotopic fractionation

Combining measurements of xylem water and leaf water with information about the Local Meteoric Water Line (LMWL) enables estimation of the average isotopic composition of local rainfall. We do this by calculating the LMWL (from δ^2H_{precip} vs $\delta^{18}O_{precip}$) using the previously published rainfall event, lake and river water data from Stansell et al. (2017). A best-fit line based on linear regression was then fitted through each leaf-xylem water isotope pair, the projection of which on the LMWL is reported as $\delta^{18}O_{LMWL}$ and δ^2H_{LMWL}. The $\delta^{18}O_{LMWL}$ was calculated by subtracting the plant leaf ($\delta^{18}O_{lw}$ and δ^2H_{lw}) and xylem ($\delta^2H_{xyl-corr}$ and $\delta^{18}O_{xylem}$) water intercept from the LMWL intercept and dividing that result with the difference in the LMWL and leaf-xylem slope values. The δ^2H_{LMWL} was calculated by multiplying the $\delta^{18}O_{LMWL}$ projection value by the slope of the LMWL line and by adding the LMWL intercept value as follows:

$$\delta^2 H_{LMWL} = \left(\frac{LMWL_{intercept} - Plant_{intercept}}{LMWL_{slope} - Plant_{slope}}\right) \times LMWL_{slope} + LMWL_{intercept} \quad (12)$$

A mean δ^2H_{LMWL} value was calculated for each species separately at either location and used as an input value in a time-series model. We use that approach instead of using the $\delta^2H_{xyl-corr}$ values to mitigate the effects of evaporation at the soil level over daily to monthly time scales. The Craig-Gordon model was then applied to hourly meteorological data (RH, T, e_a) time series during peak daylight hours (10:00 to 17:00) from April 15th 2021 to July 31st, 2021 to model leaf water δ^2H ($\delta^2H_{lw-mod-meteo}$) changes at Nuudsaku and Pangodi. Monte Carlo error ranges to the $\delta^2H_{lw-mod-meteo}$ were calculated in Excel by simulating 1000 random values using NORM.INV(RAND) function for every time series point. The input error was defined by the 1σ of mean δ^2H_{LMWL} values for each species at either location. We apply a 2-day Lowess-filter (locally weighted polynomial regression) to these data using the Origin program.

The majority of leaf waxes form during the leaf flush period following bud burst (Tipple et al., 2013). The δ^2H_{n-alk} signal in leaves tracks the local relative humidity and temperature change, yet the hydrogen is ultimately sourced from local soil water which in our case represents a compounded signal of several months of precipitation and evapotranspiration. Since we sampled the plant matter after the flush period when the leaves were mature, we constrain the leaf flush period of our sampled species in order to infer the mean leaf water δ^2H (δ^2H_{lw}) from the defined period afterwards for calculating fractionation factors between the δ^2H_{lw} and δ^2H_{n-alk}. The start of the growing season was defined by identifying the first five consecutive days of an average daily temperature above 5 °C (Krupková et al., 2017). In the year 2021, this occurred on April 15th (DOY 105) in the Pangodi and on April 16th (DOY 106) in the Nuudsaku catchment. According to the Estonian plant phenological calendar from 1949 to 1999 (Ahas, 2001), the average start date of *Sorbus aucuparia* bud burst was May 10th (1σ = 7.4 days), *Acer platanoides* on May 16th (1σ = 7.2 days) and *Quercus robur* on May 22nd (1σ = 7.7 days). However, Tooming (1996) noted that from 1953 to 1994 the average temperature at Tartu-Tõravere meteorological station rose by 4.0 °C in March and by 2.6 °C in April. Leaf development from the start of bud growth until the appearance of small leaves can take 1 to 2 months (Wesołowski and Rowiński, 2006), or in some cases even longer (Newberry et al., 2015). More specifically, a comprehensive study from Germany (Basler, 2016) showed that the mean leaf unfolding time was around five weeks. Therefore, we assumed that the leaf flush would start in late May. As the leaves had developed into full size by the first sampling date, we assumed that the leaf flush period was between late May and late June. Tipple et al. (2013) reported a two-week period during which the deciduous leaf *n*–alkanes formed and retained the δ^2H value thereafter. For defining the leaf flush period in our $\delta^2H_{lw-mod-meteo}$ data set, we used a sequential regime shift detection software (v. 6.2) with a 95 % confidence level, Huber's tuning constant of 2 and cutoff length of 50 (Rodionov, 2004). Only the regime shifts at the estimated start and end of leaf flush are reported. We then used the mean $\delta^2H_{lw-mod-meteo}$ value of each species from the time of leaf flush ($\delta^2H_{lw-mod-flush}$) at either location to calculate biosynthetic fractionation factors. Apparent fractionation (ε_{app}) was calculated between each chain length δ^2H_{n-alk} value and the mean source water δ^2H_{LMWL} at the time of leaf flush. Biosynthetic fractionation (ε_{bio}) was calculated between each chain length δ^2H_{n-alk} value and the corresponding $\delta^2H_{lw-mod-flush}$ value for each species. We also calculated the average water vapor δ^2H values during the leaf flush period ($\delta^2H_{wv-mod-flush} = \delta^2H_{xyl-corr} - \varepsilon^+$).

4. Results

4.1. Spatiotemporal variations in climatic conditions – temperature and relative humidity

In addition to the local Nuudsaku climate logger data, the Estonian Weather Service provided hourly meteorological data from 2021. Yearly precipitation amounts at Tartu-Tõravere (Pangodi) station totaled 597 mm and at Viljandi (Nuudsaku) 621 mm. The 2021 May, June, and July rainfall totals in Tartu-Tõravere were 102.7, 15.5 and 123.5 mm, and in Viljandi, 88.2, 20.3 and 111.2 mm, respectively. The most abundant rainfall at both locations occurred in July while the month with the least amount of precipitation was February (12.5 mm) at either station. Relative humidity (RH) values ranged between ~ 20 and 100 %. The daily average RH during peak sun hours on June 20th was 40 % in Tartu-Tõravere (Pangodi) and 41 % in Viljandi (Nuudsaku). On July 7th the daytime RH was higher, 55 % at Pangodi and 48 % at Nuudsaku. The 2021 air temperatures ranged between –26.2 and 33.5 °C with mean yearly temperatures 0.2 °C higher in Tartu-Tõravere (6.3 °C) than in Viljandi (6.1 °C). The lowest monthly median temperatures were in February. The highest monthly median temperatures were recorded in July, 10.3 °C at Tartu-Tõravere and 10.8 °C at the Viljandi station.

4.2. Soil and plant water

The soil water δ^2H (δ^2H_{sw}) values over the entire study period and both locations ranged from –100.4 ‰ to –43.7 ‰ and $\delta^{18}O_{sw}$ values from –13.6 ‰ to –5.2 ‰ (Fig. 3). The average δ^2H_{sw} value of all measured soil samples was –80.2 ‰, which is close to the annual average value of GNIP recorded precipitation (–79.8 ‰) from 2013 to 2018 at Tartu-Tõravere

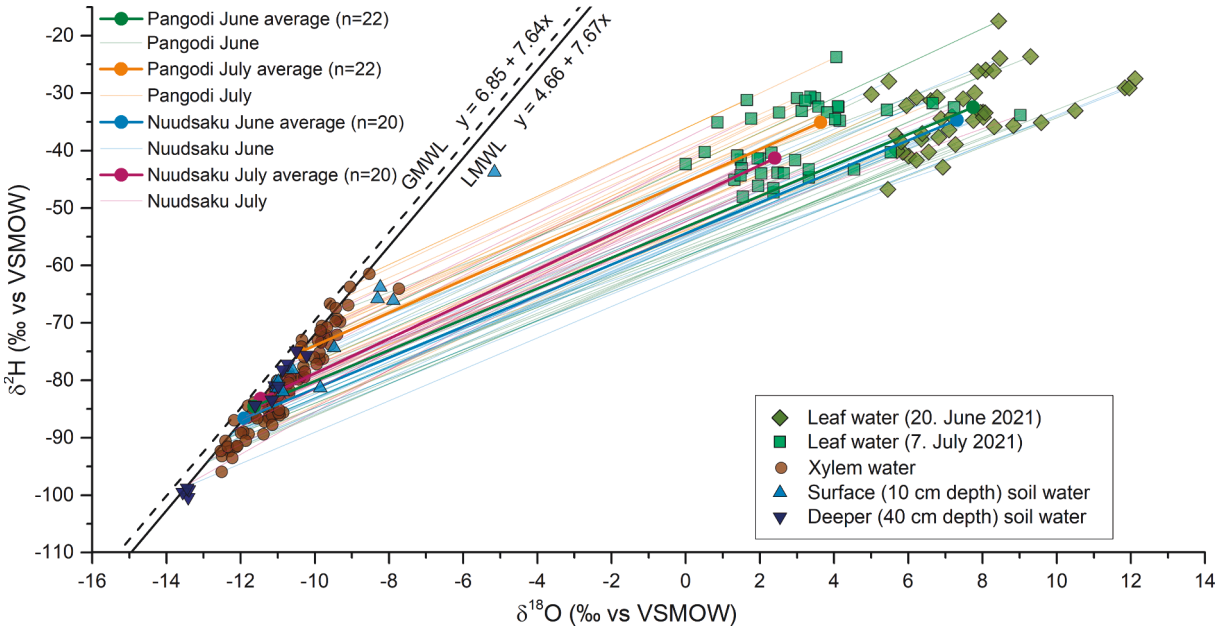

Fig. 3. Soil, leaf and (cryo-corrected) xylem water stable hydrogen (δ^2H) and oxygen ($\delta^{18}O$) isotope values at Pangodi and Nuudsaku from June and July 2021 plotted with the Local Meteoric Water Line (LMWL). The LMWL was calculated based on Estonian surface water isotope data (Stansell et al., 2017) and precipitation data (2013 – 2018) from GNIP station in Tartu-Tõravere. The global meteoric water line was adopted from Putman et al. (2019). Colored faint lines connect each individual leaf-xylem pair that extend to and are projected on the LMWL. Briefly, the $\delta^{18}O$ projection point on the LMWL was calculated by subtracting the leaf and cryo-corrected xylem water intercept from the LMWL and dividing the result with the difference in their slope values. The δ^2H projection point was acquired by multiplying the $\delta^{18}O$ projection value by the slope of the LMWL line and by adding the LMWL intercept value. Bold lines signify the average of monthly values at each location and date separately. (For interpretation of the references to colour in this figure legend, the reader is referred to the web version of this article.)

meteorological station. Relatively higher values were observed in the topmost/surface soil layer (10 cm depth), averaging (mean) at –73.7 ‰ for δ^2H_{sw} and at –9.6 ‰ for $\delta^{18}O_{sw}$. Deeper soil water profiles had lower overall mean values, –86.7 ‰ and –11.7 ‰ for δ^2H_{sw} and $\delta^{18}O_{sw}$, respectively. A 6.7 ‰ shift in the mean towards higher overall δ^2H_{sw} values (from –83.5 ‰ to –76.9 ‰) was observed between June and July measurements when the $\delta^{18}O_{sw}$ displayed a similarly small 0.7 ‰ increase (from –11.0 ‰ to –10.3 ‰). There was no statistically significant difference in soil water isotope values between the two study sites (one way ANOVA $p = 0.92$). Across all measurements, the Nuudsaku surface (10 cm depth) soil δ^2H_{sw} (–71.3 ‰) and $\delta^{18}O_{sw}$ (–9.2 ‰) mean values were slightly higher than at Pangodi (δ^2H_{sw} at –76.1 ‰ and $\delta^{18}O_{sw}$ at –9.9 ‰). Conversely, the deeper soil (40 cm) δ^2H_{sw} and $\delta^{18}O_{sw}$ at Nuudsaku were lower (δ^2H_{sw} at –88.7 ‰ and $\delta^{18}O_{sw}$ at –11.9 ‰) in comparison to Pangodi (δ^2H_{sw} at –84.8 ‰ and $\delta^{18}O_{sw}$ at –11.6 ‰).

The cryo-corrected xylem water δ^2H ($\delta^2H_{xyl-corr}$) values across all measurements ($n = 84$) ranged from –96.0 ‰ to –61.5 ‰ (median –82.5 ‰; $1\sigma = 7.9$) and $\delta^{18}O_{xylem}$ from –12.5 ‰ to –7.7 ‰ (median –10.9 ‰; $1\sigma = 1.0$; Fig. 3). The average (mean) $\delta^2H_{xyl-corr}$ values were –83.4 ‰ in June, –78.0 ‰ in July. The $\delta^{18}O_{xylem}$ averaged at –11.0 ‰ and –10.6 ‰, respectively. Nuudsaku catchment $\delta^2H_{xyl-corr}$ (–83.3 ‰) and $\delta^{18}O_{xylem}$ (–11.1 ‰) mean values were lower in comparison to values from the Pangodi catchment ($\delta^2H_{xyl-corr}$ at –78.4 ‰ and $\delta^{18}O_{xylem}$ at –10.5 ‰). *Acer platanoides* had the largest standard deviation across all measurements with $\delta^2H_{xyl-corr}$ ($1\sigma = 8.5$) ranging from –90.6 ‰ to –64.1 ‰ and $\delta^{18}O_{xylem}$ ($1\sigma = 1.2$) from –12.4 ‰ to –7.7 ‰ with the most variable results observed in the Pangodi catchment in June. The lowest variability was noted among *Alnus glutinosa* samples where $\delta^2H_{xyl-corr}$ ($1\sigma = 2.9$) varied from –76.0 ‰ to –66.9 ‰ and $\delta^{18}O_{xylem}$ ($1\sigma = 0.4$) from –10.4‰ to –9.1 ‰. The lowest $\delta^2H_{xyl-corr}$ value was recorded from *Quercus robur* (–86.6 ‰) in June and the highest from *Vaccinium myrtillus* (–69.0 ‰) xylem in July. The most notable increase in $\delta^2H_{xyl-corr}$values between two sampling dates was observed in *Alnus incana* (from –85.0 to –71.8 ‰) and *Vaccinium myrtillus* samples (from –75.5 to –62.6 ‰) at Pangodi.

The source water δ^2H and $\delta^{18}O$ values obtained from the intercept of the LMWL and the best-fit line projection of each leaf-xylem pair (δ^2H_{LMWL} and $\delta^{18}O_{LMWL}$, respectively as seen on Fig. 3) averaged at –82.3 ‰ ($1\sigma = 8.3$) and 11.3 ‰ ($1\sigma = 1.1$), respectively. The average δ^2H_{LMWL} value at Nuudsaku increased slightly from June to July (–86.7 ‰ to –83.3 ‰) and notably at Pangodi (from –84.6 ‰ to –75.2 ‰; Fig. 3). At Pangodi, the lowest mean δ^2H_{LMWL} value was observed in *Sorbus aucuparia* (–88.3 ‰) and *Quercus robur* (–86.3 ‰) with the highest in *Vaccinium myrtillus* (–69.6 ‰) values. Likewise, the mean δ^2H_{LMWL} at Nuudsaku was the lowest in *Sorbus aucuparia* (–87.8 ‰) and *Quercus robur* (–88.5 ‰), and the highest in *Alnus glutinosa* (–74.8 ‰).

Soil and xylem water δ^2H values were higher than those of co-occurring precipitation and reconstructed source water. We characterized these offsets from the LMWL by calculating the line-conditioned (LC)–excess (Landwehr and Coplen, 2006), which provides a single metric for the degree to which a water sample deviates from the LMWL in $\delta^2H/\delta^{18}O$ dual isotope space. Values below zero are indicative of kinetic isotope effects during evaporation and values above zero suggest moisture recycling, while zero or near-zero values indicate meteoric waters. The plant LC-excess values ranged from –10.4 ‰ to 2.2 ‰ (Supplemental Fig. 1). The plant LC-excess at Pangodi (mean –2.6 ‰) was 0.4 ‰ higher than at Nuudsaku (mean –3.0 ‰) over the whole study period. Comparing the two sampling dates, the mean plant LC–excess in June was –4.0 ‰ and –1.6 ‰ in July. The most prominent change between two sampling dates (4.6 ‰ increase) was observed in *Acer plantanoides* values that displayed a median LC-excess value of –4.5 ‰ in June and 0.1 ‰ in July. In most cases the mean LC-excess value increased slightly during the observation period with the exception of *Sorbus aucuparia* at Pangodi that displayed a slight decrease (1.1 ‰). The mean soil LC-excess was –2.6 ‰ at Pangodi and –3.7 ‰ at Nuudsaku. The top soil (10 cm depth) LC-excess mean value at Pangodi increased by 0.5 ‰ and decreased by 1.3 ‰ at Nuudsaku from June to July. Deep soil (40 cm depth) LC–excess at the same time increased by 2.6 ‰ at Nuudsaku and by 0.9 ‰ at Pangodi.

The measured δ^2H_{lw} ranged from –48.0 ‰ to –17.5 ‰ (mean –35.8 ‰;

$1\sigma = 6.4$) and $\delta^{18}O$ ($\delta^{18}O_{lw}$) from 0 ‰ to 12.1 ‰ (mean 5.3 ‰; $1\sigma = 2.9$; Fig. 3). The mean values from June to July δ^2H_{lw} changed from –33.5 ‰ to –38.1 ‰ while $\delta^{18}O_{lw}$ changed from 7.5 ‰ to 3.0 ‰, respectively. *Sorbus aucuparia* exhibited the lowest mean δ^2H_{lw} values (–40.7 ‰) and *Vaccinium myrtillus* the highest (–25.7 ‰). The higher (more enriched) δ^2H and $\delta^{18}O$ values for leaf water as compared to xylem, soil, or precipitation water resulted in much lower LC-excess values compared to these other waters, with leaf water LC-excess values averaging at –81.1 ‰ ($1\sigma = 19.2$; Supplemental Fig. 1). There was no significant correlation between the δ^2H_{lw} and δ^2H_{LMWL} between species means (one-way ANOVA $p < 0.00001$). The lowest $\delta^{18}O_{lw}$ values were noted in *Alnus glutinosa* samples (mean 3.8 ‰) and highest values in *Quercus robur* (mean 6.9 ‰). The fit between the measured δ^2H_{lw} and δ^2H_{lw-mod} was high (measured $\delta^2H_{lw} = 0.8206 \times \delta^2H_{lw-mod}$; $r^2 = 0.638$; $p < 0.0001$) with the linear model intercept set to 0 (Supplemental Fig. 2).

The leaf water isotopic enrichment from plant xylem to leaves ($\varepsilon_{l/x}$) was calculated from the results of 84 sample pairs. Mean $\varepsilon_{l/x}$ was 48.9 ‰ with 1σ of 7.7 (with a mean value of 54.4 ‰ in June and 43.4 ‰ in July). The highest $\varepsilon_{l/x}$ was observed in *Quercus robur* (54.0 ‰) and the lowest in *Alnus glutinosa* (43.2 ‰) values. Isotopic fractionation from soil evaporation ($\varepsilon_{x/p}$) was calculated between source water, δ^2H_{LMWL}, and $\delta^2H_{xyl-corr}$. The $\varepsilon_{x/p}$ values generally varied between –1.4 and 4.7 ‰ with an average of 1.7 ‰ (June mean 2.3 ‰ and July 1.1 ‰). The lowest $\varepsilon_{x/p}$ of 0.6 ‰ was observed in *Vaccinum myrtillus* ($n = 4$) and the highest in *Corylus avellana* at 2.7 ‰ ($n = 16$).

The mean $\delta^2H_{lw-mod-flush}$ between 28 May 2021 and 13 June 2021 (day of year (DOY) 148 and DOY 164, respectively) ranged from –44.7 ‰ to –24.9 ‰ at Pangodi and between –42.4 ‰ and –27.3 ‰ at Nuudsaku (Fig. 4). The highest mean $\delta^2H_{lw-mod-flush}$ during leaf flush was observed in *V. myrtillus* and the lowest in *S. aucuparia*. The variance (1σ) of all $\delta^2H_{lw-mod-flush}$ was <13 ‰. The $\delta^2H_{lw-mod-flush}$ time series did not exhibit spatial variability when comparing the species mean values from each site whereas only *Corylus avellana* and *Acer platanoides* values were >6 ‰ higher at Nuudsaku in comparison to Pangodi.

4.3. n-Alkane abundance and distribution in leaves

In general, *n*-alkanes between 23 and 33 carbon units in length (n-C_{23} – n-C_{33}) were detected from the leaves collected near lakes Pangodi and Nuudsaku (Fig. 5). *Acer platanoides* leaves also contained n-C_{35}, and n-C_{39} was detected in *Vaccinium myrtillus* samples. The *n*-alkane content in sampled (dry) leaves across all measurements varied between 45 and 2281 μg/g with an average of 672 μg/g (Supplemental Table 1). The mean content of n-C_{27}, n-C_{29} and n-C_{31} including all sampled leaves were 156.1, 212.5 and 175.0 μg/g, respectively. *Vaccinium myrtillus* and *Alnus incana* mean *n*-alkane content exceeded 2000 μg/g. The lowest mean values below 207 μg/g were recorded in *Corylus avellana, Alnus glutinosa* and *Quercus robur* and between 763 and 791 μg/g in *Acer platanoides* and *Sorbus Aucuparia*.

Overall, the individuals of the same species exhibited a relatively similar distribution in the *n*-alkane content (Fig. 5). The n-C_{27} was most abundant in *Alnus incana* while n-C_{29} content was highest in *Sorbus aucuparia* (>400 μg/g), *Vaccinium myrtillus* (>400 μg/g) and *Alnus incana* (>1150 μg/g). High amounts of n-C_{31} were detected in *Acer platanoides* (>400 μg/g) and *Vaccinium myrtillus* (>800 μg/g). Most of the *Acer platanoides* individual *n*-alkanes ranged from 0 to 165.6 μg/g except for n-C_{31} that varied between 357.8 and 745.3 μg/g. The two dominant compounds in *Alnus incana* leaves were n-C_{27} (1092.3 – 1292.1 μg/g) and n-C_{29} (564.8 – 741.9 μg/g). *Sorbus aucuparia* n-C_{29} content was the highest across all species and highly variable (99.9 to 1021.9 μg/g). *Corylus avellana, Alnus glutinosa* and *Quercus robur* exhibited the lowest values with each individual *n*–alkane content reaching no more than 157.3 μg/g. The n-C_{31} content was the highest (741.0 – 1035.2 μg/g) in *Vaccinium myrtillus* at Pangodi. The second most dominant compound in *Vaccinium myrtillus* leaves was n-C_{29} (462.1 – 475.1 μg/g).

The carbon preference index (CPI) showed a strong odd-over-even predominance in *Alnus incana* (mean CPI 40.2) and *Sorbus aucuparia* (mean CPI 29.2). The mean CPI was the lowest at 8.6 for *Acer platanoides* and varied between 13.45 and 16.1 for the rest of the species (Fig. 5, Supplemental Table 1). The mean CPI of all Pangodi samples was 26.5 in June and 17.8 in July. Nuudsaku samples also showed a decrease in the CPI from 15.9 in June to 14.8 in July. All species showed a slight increase (< 0.6) in the average chain length (ACL) of *n*-alkane mean values at both sites from June to July except for *Vaccinium myrtillus* (ACL decreased by 0.2). The overall ACL increased at both Nuudsaku (from 28.7 to 29.0) and Pangodi (from 28.9 to 29.1). *Acer platanoides* and *Vaccinium myrtillus* had the highest overall ACL (31.0 and 30.2, respectively), followed by *Corylus avellana* and *Sorbus aucuparia* (29.3 and 29.1, respectively). *Alnus glutinosa*, *Alnus incana* and *Quercus robur* ACL values were between 27.0 and 27.8. Based on the peak area calculations in the GC, the average ACL in the surface sediment was 27.1.

4.4. δ^2H values of leaf-derived n-alkanes

The δ^2H_{n-alk} values were measured from chain lengths that were abundant enough for isotopic analysis. The mean δ^2H_{n-alk} values of each chain length *n*–alkane from all measurements between the Nuudsaku and Pangodi sites were similar (<10 ‰ difference in δ^2H values; Supplemental Table 2 and Fig. 6) and were in the range of –214 to –116 ‰. Slightly higher mean values were noted in δ^2H_{C29-33} with respect to δ^2H_{C23-27}. The combined δ^2H_{n-alk} values from all plant measurements averaged at –168 ‰ ($1\sigma = 18$), showing a relatively consistent distribution between sites and within the sediment. The inter-species standard deviation of δ^2H_{n-alk} values within each chain length group was generally <11 ‰ with higher variability (1σ) noted in *Alnus glutinosa* δ^2H_{C27} (16 ‰) and δ^2H_{C29} (23 ‰), *Sorbus aucuparia* δ^2H_{C31} (18 ‰), and *Vaccinium myrtillus* δ^2H_{C27} (31 ‰) and δ^2H_{C29} (24 ‰). Comparison of δ^2H_{n-alk} between the sampling sites exhibited an average of 4 ‰ difference with the exception of *Sorbus aucuparia* that had 14 ‰ lower δ^2H_{C29} and 21 ‰ lower δ^2H_{C31} values at Pangodi, most likely due to the larger size of *S. aucuparia* trees at that site. Overall, the lowest plant δ^2H_{n-alk} were noted in *Alnus glutinosa* and the highest in *Vaccinum myrtillus* (Fig. 6). There was no significant difference between surface sediment δ^2H_{n-alk} values from Nuudsaku and Pangodi (one-way ANOVA $p = 0.55$, $n = 5$).

4.5. Hydrogen isotopic fractionation between water and n-alkanes (ε_{bio} and ε_{app})

Modeled average leaf water values from the leaf flush period were used to calculate the biosynthetic isotopic fractionation (ε_{bio}) between the δ^2H_{lw} and δ^2H of each *n*-alkane (Fig. 7). The lowest (most negative) biosynthetic isotope fractionation, implying the largest absolute ε_{bio} value, was observed in n-C_{27} (median –141 ‰) at Pangodi, and in n-C_{25} at Nuudsaku (median –142 ‰). The highest (least negative) isotope fractionation indicating the smallest absolute ε_{bio} values occurred in n-C_{33} at both locations (Fig. 7). Comparison between each species ε_{bio} values at either location showed the greatest difference in *A. platanoides* *n*–C_{31} (26 ‰), *n*–C_{33} (25 ‰) and *S. aucuparia* *n*-C31 (19 ‰). The ε_{bio} at Pangodi was on average 11 ‰ smaller than at Nuudsaku when comparing the same species (Fig. 7 panels a and b). The average overall ε_{bio} across all measurements was –132 ‰ ($1\sigma = 19$). The range in the mean ε_{bio} values between all seven species was 49 ‰ and 39 ‰ among trees. The difference between combined Pangodi (–133 ‰, $1\sigma = 17$) and Nuudsaku (–131 ‰, $1\sigma = 22$) ε_{bio} values is relatively small and these combined results between the sites are not significantly different (one-way ANOVA $p = 0.52$). Apparent fractionation (ε_{app}) between δ^2H_{LMWL} and δ^2H_{n-alk} ranged from –105 ‰ in n-C_{29} and –90 ‰ in n-C_{33} at Pangodi, and between –100 ‰ in n-C_{25} and –62 ‰ in n-C_{33} at Nuudsaku. The average ε_{app} including all measurements from both locations was –93 ‰ ($1\sigma = 21$). Modeled water vapor δ^2H

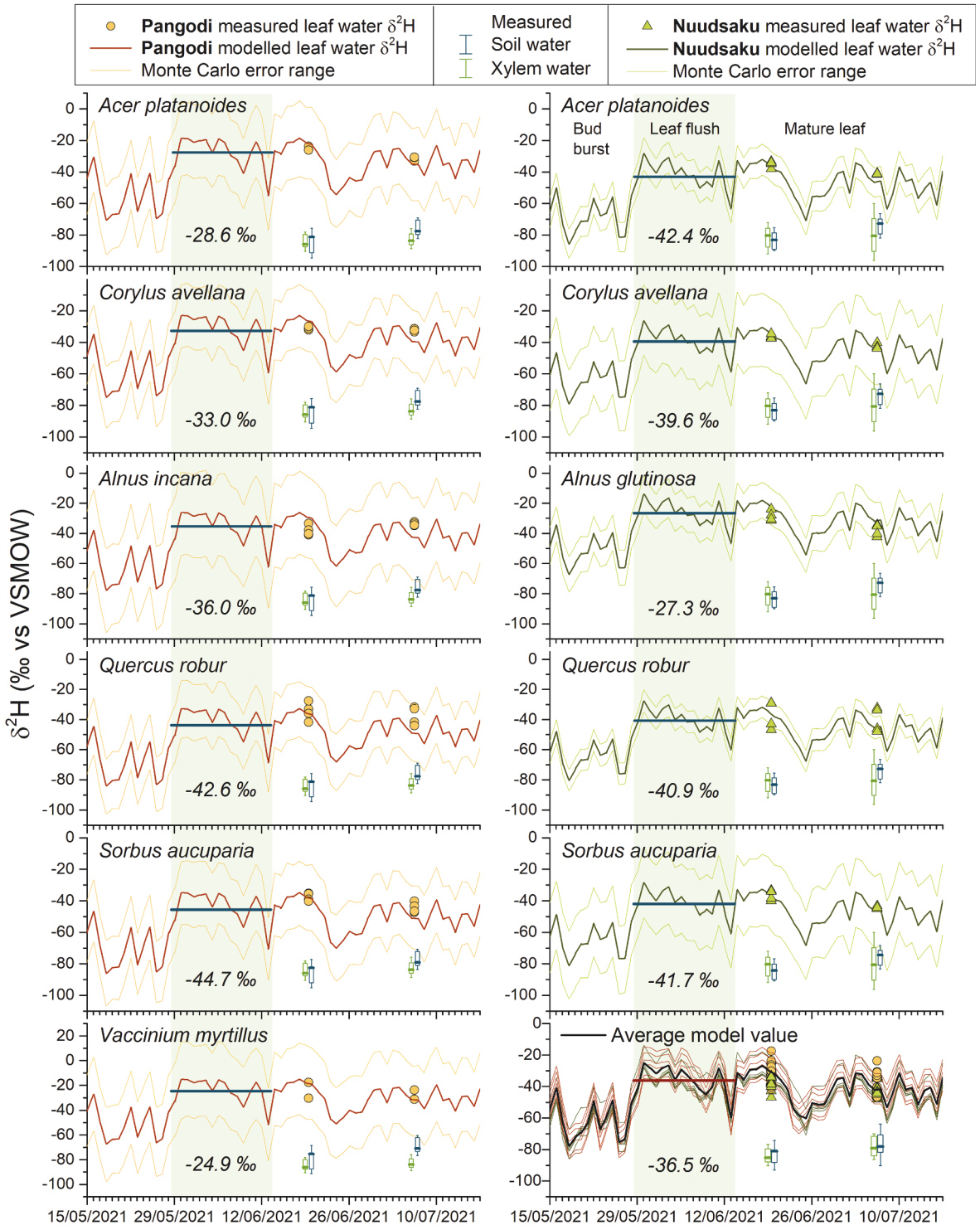

Fig. 4. Modeled mean daily leaf water δ^2H variability (Lowess two-day filter) in *Acer platanoides*, *Corylus avellana*, *Quercus robur* and *Sorbus aucuparia* at both Pangodi (orange bold line) and Nuudsaku (green bold line) locations, *Vaccinium myrtillus* and *Alnus incana* at Pangodi and *Alnus glutinosa* at Nuudsaku. Faint orange and green lines represent Monte Carlo error ranges from 1000 runs on every data point. Box plots on every sub-panel represent soil (blue) and corrected xylem (green) water δ^2H values from either location on both sampling dates with boxes extending to 25th and 75th percentiles; middle lines represent median values and whiskers represent the 1σ range (Nuudsaku July n = 20 and June n = 20; Pangodi June n = 22 and July n = 22). Bottom right plot shows all modeled and measured values from other panels overlain by the model mean (black line). The average leaf water δ^2H value from leaf flush period ($\delta^2H_{lw-mod-flush}$) is written in the green section of each individual panel, and shown as a dark blue line in the green sections. The average model value in the bottom right panel is highlighted in dark red. (For interpretation of the references to colour in this figure legend, the reader is referred to the web version of this article.)

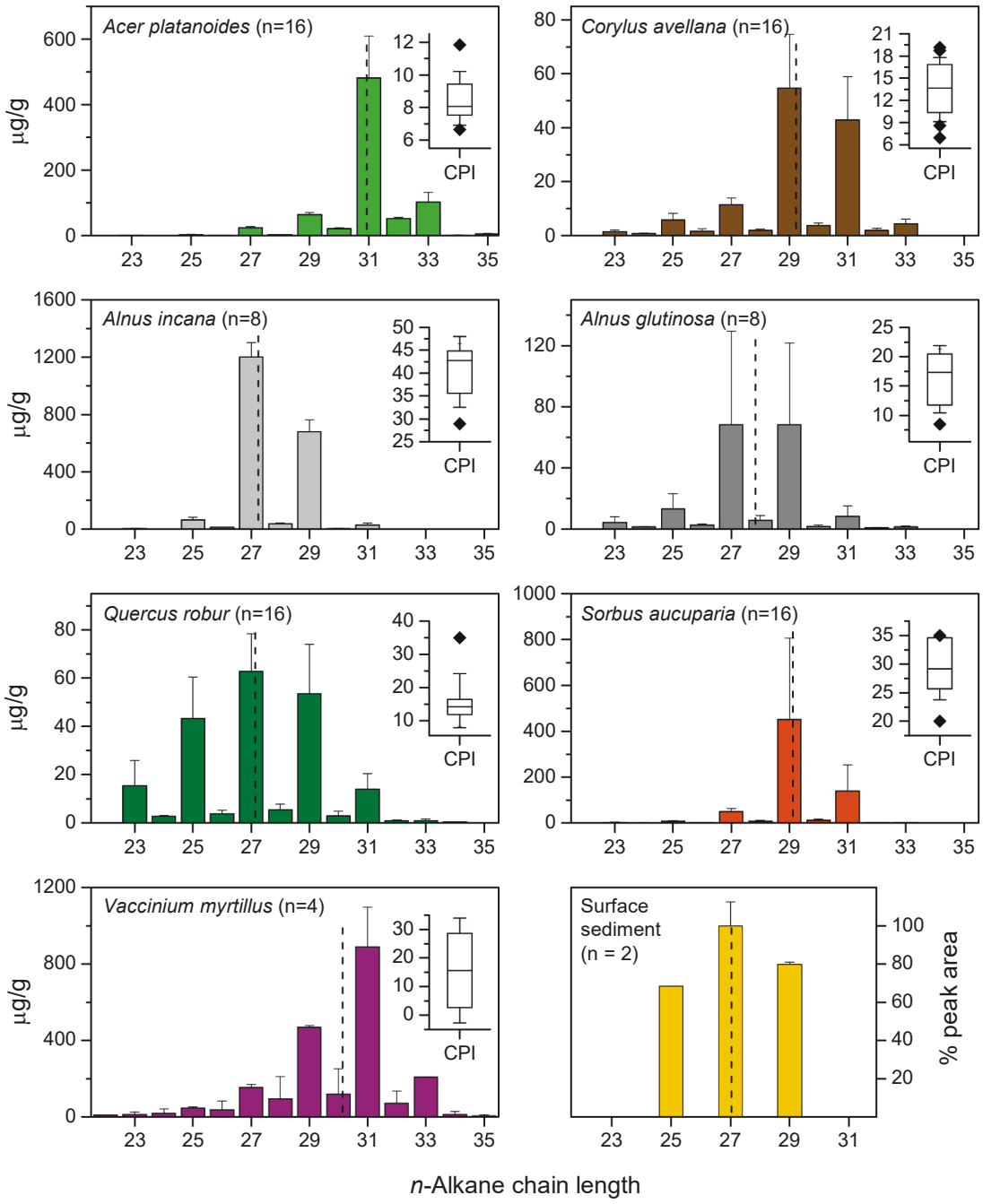

Fig. 5. The content of *n*-alkanes (*n*-C_{22} – *n*-C_{35}) in µg/g (per dry leaf) from seven species and surface lake sediment collected at Nuudsaku and Pangodi, Estonia, with the exception of *Vaccinium myrtillus* and *Alnus incana* only from Pangodi and *Alnus glutinosa* from Nuudsaku. Surface sediment *n*-alkane abundance is derived from the δ^2H_{n-alk} peak area of the gas chromatographs, normalized to the most abundant compound. Error bars in main panels represent one standard deviation (1σ) of the mean values and the number n in parenthesis is the total number of samples per given species/sediment. Average chain length (ACL) calculated from *n*-C_{23} – *n*-C_{35} content is marked in each panel as vertical dashed line. A carbon preference index (CPI) was calculated for each species from *n*-C_{24} – *n*-C_{34} alkanes. The boxes in the upper right corner of subpanels represent CPI with 25th and 75th percentiles as boxes, middle lines are medians and whiskers extend to 1σ. Outliers are marked by diamond symbols.

($\delta^2H_{wv-mod-flush}$) mean values from the leaf flush period were –163 ‰ (1σ = 4) at Pangodi and –170 ‰ (1σ = 4) at Nuudsaku. The mean δ^2H_{LMWL} was –85 ‰ at Nuudsaku and –80 ‰ at Pangodi.

4.6. Leaf water enrichment

The δ^2H_{n-alk} ^{2}H-enrichment over leaf water can be determined by calculating the slope between $\varepsilon_{leaf/LMWL}$ and ε_{app} (Kahmen et al., 2013a). This approach estimates the extent of leaf water ^{2}H–enrichment contributing to the biosynthetic water pool by quantifying the degree by which the δ^2H_{n-alk} are affected. For all species represented by 4 or more samples in our study, the slope values including all chain lengths were 1.11 ± 0.38 for *Acer platanoides*, 0.39 ± 0.48 for *Corylus avellana*, 0.32 for *Alnus incana* (±0.56) and *Quercus robur* (±0.27), 1.44 ± 0.71 for *Sorbus aucuparia* and 1.26 ± 0.74 for *Alnus glutinosa* (Supplemental Fig. 3). Comparing the two locations, the slope was 1.59 ± 0.34 for Nuudsaku and 0.41 ± 0.23 for Pangodi. Comparing different chain lengths, the slope values for *n*-C_{23} and *n*-C_{25} alkanes were negative

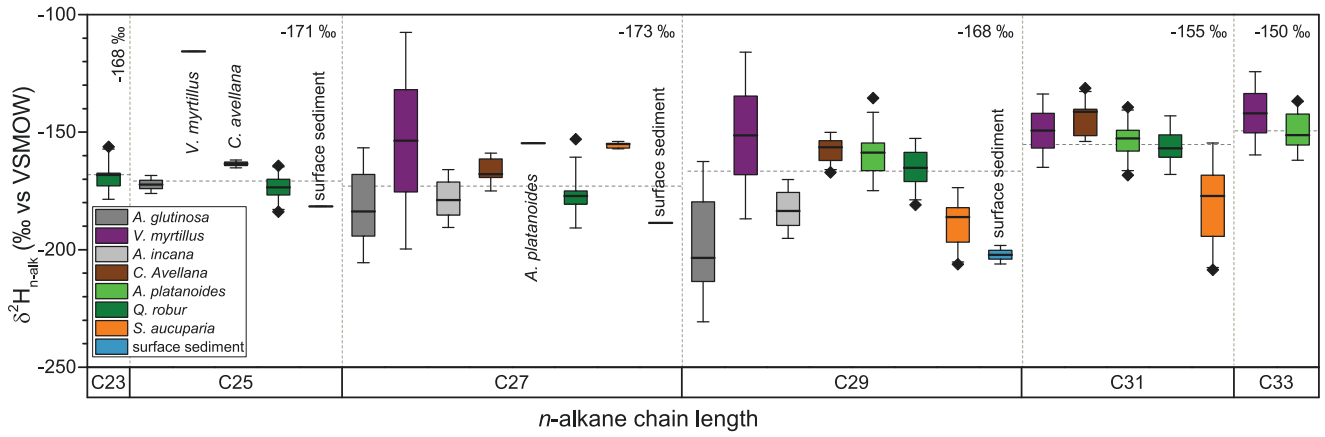

Fig. 6. $\delta^2H_{n\text{–alk}}$ values from all species in both studied lake catchments: *Acer platanoides* (n = 16), *Corylus avellana* (n = 16), *Quercus robur* (n = 16), *Sorbus aucuparia* (n = 16), *Vaccinium myrtillus* (n = 4), *Alnus incana* (n = 8) and *Alnus glutinosa* (n = 8). Surface sediment derived $\delta^2H_{n\text{–alk}}$ values are from Lake Nuudsaku (n = 1) and Lake Pangodi (n = 1). Boxes represent quartiles, middle lines are median values, the whiskers mark 1.5 σ with symbols as outliers. Horizontal gray dashed lines in each *n*–alkane chain length section mark the median $\delta^2H_{n\text{–alk}}$ value of all plant samples in group, also written in the top right corner of each sub-panel. (For interpretation of the references to colour in this figure legend, the reader is referred to the web version of this article.)

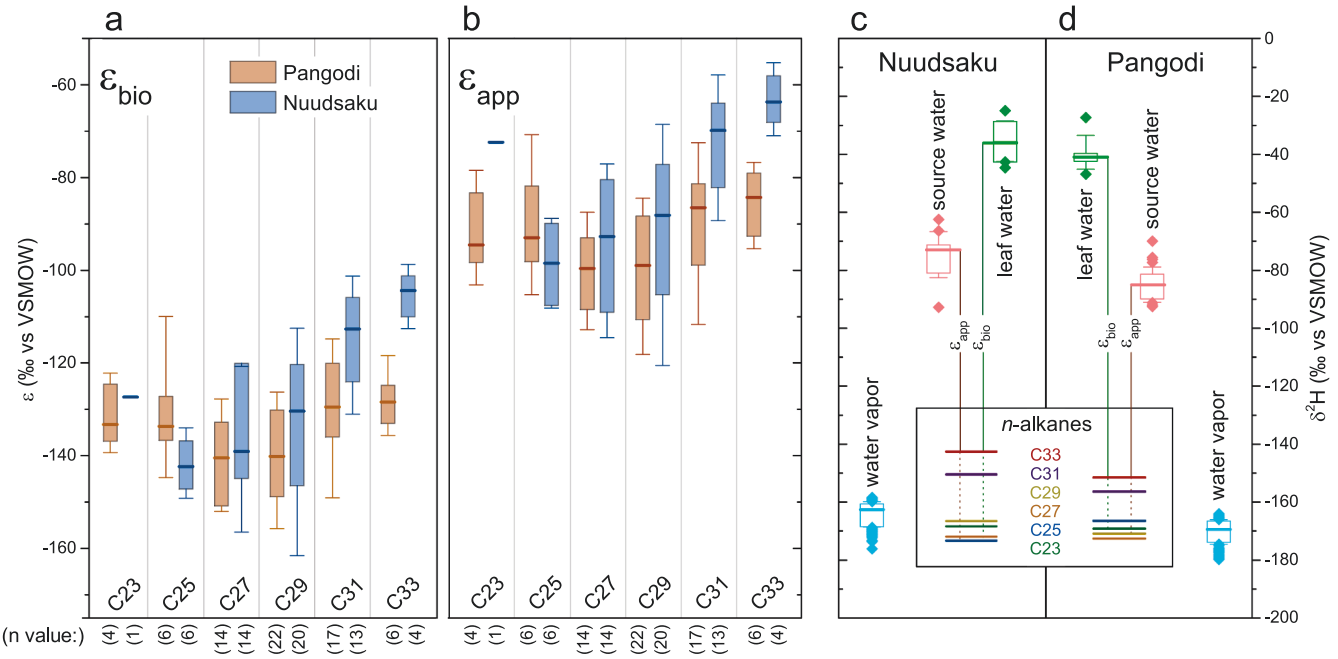

Fig. 7. Biosynthetic fractionation (ε_{bio}; a), apparent fractionation (ε_{app}; b), plant leaf derived δ^2H values of odd-chain *n*–alkanes plotted all together for *Acer platanoides*, *Corylus avellana*, *Quercus robur*, *Sorbus aucuparia and Alnus glutinosa* at Nuudsaku (c) and *Acer platanoides*, *Corylus avellana*, *Quercus robur*, *Sorbus aucuparia*, *Vaccinium myrtillus* and *Alnus incana* at Pangodi (d). The n values of the ε_{bio} and ε_{app} are written below the panels in parentheses. Modeled leaf water (n = 84) and water vapor δ^2H combined values from the time of leaf flush during peak sun hours are shown on the right panels (c and d). Source water box represents the leaf-xylem water line δ^2H intercept value on the LMWL (δ^2H_{LMWL}; n = 84). Boxes represent quartiles, middle lines are median values, the whiskers mark 1σ range and symbols are outliers. (For interpretation of the references to colour in this figure legend, the reader is referred to the web version of this article.)

(–0.25 ± 0.59 and –0.66 ± 0.48, respectively), below 1 for *n*-C_{27}, *n*-C_{31} and *n*-C_{33} (0.65 ± 0.38, 0.60 ± 0.48 and 0.53 ± 0.61, respectively), and above 1 for *n*-C_{29} (1.06 ± 0.38). The ε_{app} and $\varepsilon_{leaf/LMWL}$ in our study are poorly, yet significantly correlated ($r^2 = 0.24$). Measurements across all measurements resulted in a slope of 0.93 ± 0.22 (Supplemental Fig. 3).

5. Discussion

5.1. Soil and plant water isotope dynamics

Soil and xylem water isotope values show that plant source waters in our study locations are largely meteoric, and differences between plant water and precipitation δ^2H values are primarily driven by temporal integration in the soil column (Fig. 3 and Supplemental Fig. 1). Although minor evaporative effects can be observed in some soil and xylem samples, these are for the most part small, indicating that the isotopic signal is not greatly impacted by post-depositional alteration. Deeper soil water at high latitudes is usually lower in ^2H and ^{18}O than shallow soil water during the growing season (Amin et al., 2020) due to the seasonality of recharge by precipitation (Vargas et al., 2017; Sprenger et al., 2018). The mean δ^2H_{sw} in the upper soil layers (–74 ± 10 ‰) and $\delta^2H_{xyl\text{–}corr}$ (–81 ± 8 ‰) values in our study were slightly higher than the deep soil water (–87 ± 10 ‰), indicating that the plants in our study mainly draw their water from the upper 40 cm soils. We found no

statistical difference in $\delta^2H_{xyl-corr}$ values between the two sampling dates in June and July. This suggests that the plant source water did not significantly vary throughout the vegetation period, which has also been observed in other studies (Kahmen et al., 2013a).

The shift in LC–excess value can be used as a tracer for changes in plant water uptake (Flanagan et al., 2019). The bulk soil water values in this study were mostly in the range of plant xylem LC-excess (Supplemental Fig. 1). The LC-excess differences between soil profiles revealed that the water in the upper soil profiles (10 cm, –4.9 ± 3.7 ‰) was slightly (3.5 ‰) more isotopically enriched than at deeper depth (40 cm, –1.4 ± 1.7 ‰). This suggests that the largest degree of evaporative enrichment occurs in the shallow (10 cm depth) soils. The deep soil LC-excess (–1.4 ± 1.7 ‰) was in the range of model simulated (Piso.AI) values from 2004 to 2020 (–1.0 ± 4.3 ‰; one-way ANOVA, $p = 0.77$) as well as the LC-excess calculated from GNIP measurements at Tartu-Tõravere from 2013 to 2018 (0.8 ± 3.9 ‰; one-way ANOVA, $p = 0.40$), suggesting that the conditions that were encountered during this study period are characteristic of those over the recent past. This also suggests the plants have a consistent access to soil water that does not likely change to the degree which can be observed in plant leaf δ^2H_{lw} values (Kahmen et al., 2013a).

Near-zero LC-excess values indicate access to deeper water as evaporation results in lower LC-excess that can be observed in shallow soil profiles (McCutcheon et al., 2017). *Vaccinium myrtillus* and *Corylus avellana* roots mostly reside in the topmost soil profile, explaining relatively enriched root water isotope values (Fig. 4). *Sorbus aucuparia* at Pangodi was one of the largest trees sampled explaining its lowest overall xylem water isotope values, although the LC-excess also likely displays the species susceptibility to dryness (Supplemental Fig. 1). A study by Lauteri et al (2006) demonstrated that *C. avellana* shrubs are capable of drawing from both relatively shallow (enriched) and deep (depleted) soil water depending on water availability. The *C. avellana* shrub in our study notably follows that trend (Supplemental Fig. 1) with the LC-excess across all measurements decreasing by 3 ‰ between the two sampling dates. We attribute the largest ~ 5 ‰ increase in *Acer platanoides* LC-excess from June to July at both sites to increased sensitivity to soil evaporation dynamics because the species values approach those found in shallow soil. The general increase in LC-excess values suggests that the plants likely accessed deeper soil waters between the two sampling dates due to the dry period. These differences, although informative, are small, indicating that the plant water inputs are relatively consistent over time and between species, and not greatly impacted by evaporative effects at the soil surface.

5.2. Leaf water enrichment

Leaf water ^2H-contribution to the biosynthetic water pool was quantified by calculating the slope value between ε_{app} and $\varepsilon_{leaaf/LMWL}$ (Supplemental Fig. 3). Our reported slope of 0.93 from all measurements suggests that the ^2H–enriched leaf water contributes 93 % overall to the biosynthetic water pool of the species studied and that the leaf water enrichment (instead of soil water evaporation) is the main driver of plant δ^2H_{n-alk} values, which ultimately reflect the δ^2H_{lw} values. The model values greater than 1 most likely indicate a 100 % contribution from leaf water. The uncertainty associated with the model may also arise from the water vapor δ^2H ($\delta^2H_{wv-mod-flush}$) values which are merely calculated estimates. Another possibility for explaining the overestimation could be the low range in ε_{app} and $\varepsilon_{leaf/LMWL}$ estimates or a temporal mismatch between the δ^2H_{precip} and δ^2H_{n-alk}. Kahmen et al., (2013a) associate the over 100 % leaf water contribution with analytical errors and variability in the biology of the species. Overall, our study demonstrates that the leaf water ^2H-enrichment over δ^2H_{n-alk} does differ comparing the two catchments, and that the alkane-specific slopes suggest a 100 % contribution by the *n*–C_{29} compound.

5.3. Isotopic fractionation from leaf transpiration ($\varepsilon_{l/x}$) and soil evaporation ($\varepsilon_{x/p}$)

Leaf water ^2H-enrichment above xylem water ($\varepsilon_{l/x}$) is a key parameter in understanding the effect of transpiration on leaf δ^2H_{n-alk} values (Feakins and Sessions, 2010). The mean $\varepsilon_{l/x}$ in our study from all measurements is 48.9 ± 7.7 ‰, which indicates that leaf transpiration has been relatively stable during the sampling period. These results are also in an agreement with the global angiosperm $\varepsilon^2H_{l/x}$ model by Kahmen et al. (2013a). Our reported results are lower than in an arid region (Feakins and Sessions, 2010), yet higher than that of reported in the higher latitude regions (Daniels et al., 2017; Berke et al., 2019).

Xylem water $\delta^2H_{xyl-corr}$ enrichment above precipitation water δ^2H_{LMWL} ($\varepsilon_{x/p}$) could be an important part of ε_{app} in some settings (Sachse et al., 2012). The species mean $\varepsilon_{x/p}$ values in our study were significantly different (one way ANOVA $p = 0.03$) which indicates that plant morphology plays an important role in shaping the ε_{app} values. However, the overall $\varepsilon_{x/p}$ variability in our data was relatively small, –1.7 ‰ ($1\sigma = 2.5$), and falls within the previously published $\varepsilon_{x/p}$ range of –1 ± 13 ‰ by Feakins and Sessions (2010). The catchments in our study do not therefore display a significant uptake of ^2H-enriched soil waters. Applying a one-sample T-test shows that the Feakins and Sessions (2010) $\varepsilon_{x/p}$ values are not significantly different from that of ours.

5.4. Leaf wax n-alkane distribution, abundance, potential sources and δ^2H values

Studying plants within lake catchments can help to improve paleohydrology reconstructions from sedimentary plant waxes. In particular, the ACL and CPI of the plants are indicators of changes related to the surrounding environment and type of vegetation (Balascio et al., 2018b) as terrestrial plants generally have a higher ACL than aquatic taxa (Sachse et al., 2012). Although we sampled a limited range of species, the average ACL (28.9) and the observed chain length distributions (Fig. 5) demonstrate that the *n*-C_{29} alkane is the dominant chain length in our data, as has often been observed in temperate deciduous species (Bush and McInerney, 2013). This distribution suggests that the *n*-C_{29} alkane would be an appropriate biomarker for inferring source water signal, which is primarily controlled by relative humidity-driven transpiration at the plant leaf level without any major effect of relative humidity-driven evaporation from the soil.

Lake Nuudsaku and Lake Pangodi surface sediment *n*-alkane content shows *n*-C_{27} as the most abundant, and *n*-C_{29} the second most abundant alkane; *n*-C_{25} was the third most dominant compound only detected in lake Pangodi sediments (Fig. 5). Regardless, our plant *n*-alkane content shows that the *n*-C_{29} alkane is still the most abundant compound found in the leaves and should therefore be the most contributing chain length to lake sediments. In addition, the plants produce high amounts of *n*-C_{31} that we did not detect in the lake sediments. This difference may arise from either the abundant alkane input from other species around the lakes that we did not sample, or possibly from leaf litter degradation by microbes before deposition in the lake (Zech et al., 2011). The mean *n*-alkane abundance of *n*-C_{27}, *n*-C_{29} and *n*-C_{31} (156.1, 212.5 and 175.0 μg/g, respectively) including all sampled species was in a general agreement of previously reported angiosperm range by Diefendorf et al. (2011). *Alnus incana*, *Sorbus aucuparia* and *Vaccinum myrtillus* have the highest overall *n*-alkane content out of the seven sampled species, indicating that these species have a higher likelihood of driving the δ^2H_{n-alk} signal in the lake sediments. We also found that the *n*-alkane production in our sampled species (Fig. 5) overlaps those reported by Bush and McInerney (2013).

The δ^2H_{n-alk} values in our study show relatively modest variability (–167 ± 18 ‰; Fig. 6) and are in the range of modern leaf wax values observed in other mid and high–latitude terrestrial plants (Feakins and Sessions, 2010; Sachse et al., 2012; Liu and An, 2019), and as expected, slightly higher than in the Arctic (Daniels et al., 2017; O'Connor et al.,

2020). Our sedimentary δ^2H_{n-alk} values are lower in comparison to the plant wax δ^2H_{n-alk}. For example, comparing only our δ^2H_{C29} values from leaf waxes and sediments results in an offset of –37 ± 22 ‰. Sachse et al. (2006) associate a similar finding with high ^2H–enrichment during the summer months with the possibility of biosynthesis in the leaves continuing until the fall. The offset in our data set could additionally be explained by the fact that we only sampled a limited number of species. Furthermore, a considerable grass input to the lakes could decrease the sedimentary δ^2H_{C29} value up to 34 ‰ (Sachse et al., 2012). Calculating the mean weighted average δ^2H_{n-alk} of the surface sediment based on the Lake Pangodi pollen percentages (25 % broad and 22 % needle leaved trees, 2 % shrubs, 34 % herbs and 17 % grasses with the lowest (most negative) reported isotopic values of –167 ‰ (from this study), –110 ‰, –118 ‰, –147 ‰ and –147 ‰ (from Sachse et al., 2012), respectively) results in a –142 ‰ average for the surface-most sediment, which is 25 ‰ higher than our modern leaf waxes (–167 ‰), and 51 ‰ higher when comparing to the mean measured sedimentary δ^2H_{n-alk} (–193 ‰). Nonetheless, we find the leaf wax lipid distributions and δ^2H_{n-alk} values relatively consistent between sites and with the sediment, implying that these are major sources to the sediments.

5.5. Hydrogen isotope fractionation between source water, leaf water and n-alkanes (ε_{app}, ε_{bio})

Leaf water δ^2H_{lw} values represent a combined signal of δ^2H_{precip}, air temperature and relative humidity, making it a useful parameter for tracing hydroclimate changes (Farquhar et al., 2007). However, since the δ^2H_{lw} constantly changes in response to shifting climate conditions, lack of local information of the source water (δ^2H_{LMWL}) and leaf wax δ^2H_{n-alk} (ε_{app}) increases the uncertainty of paleo-hydrological reconstructions (Sachse et al., 2012). The ε_{app} is an intrinsically complex measure due to variable environmental conditions and plant physiology. Our average ε_{app} values calculated from the *n*-alkanes from all species in this study are presented in Table 1. These values fall in the range of previously reported ε_{app} from other regions (Sachse et al., 2006, 2009, 2012; Balascio et al., 2018a; Berke et al., 2019). The average ε_{app} calculated from all *n*-alkanes and the individual δ^2H_{LMWL} in our study was –93 ± 21 ‰ (1σ, n = 42). We find a negligible 1 ‰ difference between the latter and the ε_{app} calculated from the average annual δ^2H_{precip} of ~ –80 ‰ from 2013 to 2018 (IAEA, 2022), which is –92 ± 21 ‰ (Fig. 8), suggesting that the readily available annual δ^2H_{precip} is an appropriate variable for calculating the ε_{app} at our study location. Our ε_{app} overlaps the reported ε_{app} mean species value of –94 ± 21 ‰ by Feakins and Sessions (2010), –89 ± 28 ‰ by O'Connor et al. (2020) and –89 ± 14 ‰ by Daniels et al. (2017). The ε_{app} calculated from our δ^2H_{C29} (and δ^2H_{LMWL}) is –99 ± 21 ‰ and falls within the error range of the mean high-latitude angiosperm ε_{app} of –119 ± 29 ‰ by Liu et al. (2016), the data from which were later included in the global plant-scale data set mean values of –116 ± 5 ‰, reported by Liu and An (2019), also calculated from δ^2H_{C29} values (Fig. 8). When comparing the *sedimentary* mean δ^2H_{n-alk} (δ^2H_{C29} = –202 ‰, δ^2H_{C27} = –189 ‰ and δ^2H_{C25} = –182 ‰) in our study and the modern mean yearly δ^2H_{precip} values, these yield an ε_{app} values of –133 ‰, –118 ‰ and –110 ‰, respectively, which have larger absolute values than the ε_{app} calculated from our plant leaves (–93 ± 21 ‰). The lowest calculated value falls within the range of the 1σ error of the ε_{app} which likely incorporates leaf water ^2H–enrichment during the leaf formation period (Sachse et al., 2006).

Plant water usage as well as physiological and biosynthetic differences can affect the fractionation values. For example, the sedimentary record may incorporate the isotopically depleted signal of aquatic plants (Liu and An, 2019). The ε_{bio} is a species-specific measure that is calculated between the biosynthetic source water pool δ^2H value, which we take here from the mean modeled leaf water $\delta^2H_{lw-mod-flush}$, and the δ^2H_{n-alk} value of lipids synthesized from this hydrogen source. In this study, the average ε_{bio} including all species and measurements was –132 ‰ (1σ = 19); the average ε_{bio} values for individual chain lengths from all species are shown in Table 1. We report the largest absolute ε_{bio} values (–139 ‰) calculated from both *n*-C_{27} and *n*-C_{29} alkanes. Although ε_{bio} has been suggested to vary in some compounds in response to extreme metabolic stress (Cormier et al., 2018; Baan et al., 2023), it is less likely to vary over time (in contrast to ε_{app}) and can thus facilitate application in sediment cores from these sites to reconstruct mean site leaf water δ^2H values in the past. Our ε_{bio} has therefore implications for quantitatively reconstructing leaf water δ^2H, which enables estimating past relative humidity changes through leaf water modeling.

5.6. Implications for paleo-hydrological reconstruction

We set up this study to understand the relationship between the δ^2H_{n-alk} values and biosynthetic water pools in two different catchments. No single measurement of the plant biomass could characterize the basin-wide fractionation factors, however, sampling a variety of common trees and shrubs has proven useful (Sachse et al., 2006; Berke et al., 2019; McFarlin et al., 2019). It has been noted that the ε_{app} on a global scale is still a major area of uncertainty (Sachse et al., 2012; Konecky et al., 2019), and the ε_{app} decreases with increasing latitude. This suggests that the ε_{app} value likely has a smaller absolute value where strong evaporative conditions prevail as our reported ε_{app} of –99 ± 20 ‰ is below the global average of –116 ± 5 ‰ (Liu and An, 2019), both of which were calculated from δ^2H_{C29} values (Fig. 8). Our average ε_{bio} (–132 ± 19 ‰) is larger in comparison to a study from Greenland (–120 ‰; 1σ = 27; Berke et al., 2019), yet smaller than ε_{bio} of field-based measurements from California, USA (–149 ‰; 1σ = 16) by Feakins and Sessions (2010). The ε_{app} includes a temperature and RH component which is expected to change with latitude. The differences in the ε_{app} are also related to differences in plant species or adaptions. Our sediment δ^2H_{n-alk} profile may include shifts in species distribution in the catchment area that could impact the mean sedimentary ε_{bio} (Freimuth et al., 2019). However, we found that across the sampled major leaf wax producing species in our studied lake catchments, that ε_{bio} values were consistent between locations despite slight differences in the distributions of species living in the catchment (Fig. 7, Table 1). The ε_{app} values in our study between the two sites were also similar, and comparable with values from previously reported estimates (Fig. 8).

Potential changes in paleo-vegetation may be partially detected through available pollen data and from changes in the distribution patterns of *n*-alkanes present in the sediments (Feakins, 2013). For example, if *Alnus incana* (ACL 27.7) and *Quercus robur* (ACL 27.1) were to become less widespread in the catchment area while *Acer platanoides* (ACL 31.0) and *Vaccinum myrtillus* (ACL 30.2) abundance was increasing then the lake sediment *n*-alkane composition would shift towards a higher ACL of the vegetation (Fig. 5). Each of these species also has a different CPI which would in this particular case result in a shift towards a lower CPI in the sediments. However, plant waxes are not equally sourced from biomass, therefore interpreting the distribution of *n*-alkanes could highly benefit from additional proxies (such as pollen, which could help understand the species composition of sediment) for a paleo-hydrological reconstruction (Sachse et al., 2006). In the case of Lake Pangodi, the pollen data (Palusalu et al., 2023) support previous

Table 1
Apparent (ε_{app}) and biosynthetic (ε_{bio}) fractionation calculated from seven plant species (n = 42) at Pangodi and Nuudsaku. The reported ε_{app} values are calculated between the respective δ^2H_{n-alk} and mean annual δ^2H_{precip} of –80 ‰.

n–alkane	ε_{bio} (‰)	1σ	ε_{app} (‰)	1σ
n–C_{23}	–130	8	–95	7
n–C_{25}	–135	15	–95	19
n–C_{27}	–139	15	–98	15
n–C_{29}	–139	20	–99	20
n–C_{31}	–125	18	–85	20
n–C_{33}	–119	13	–74	10

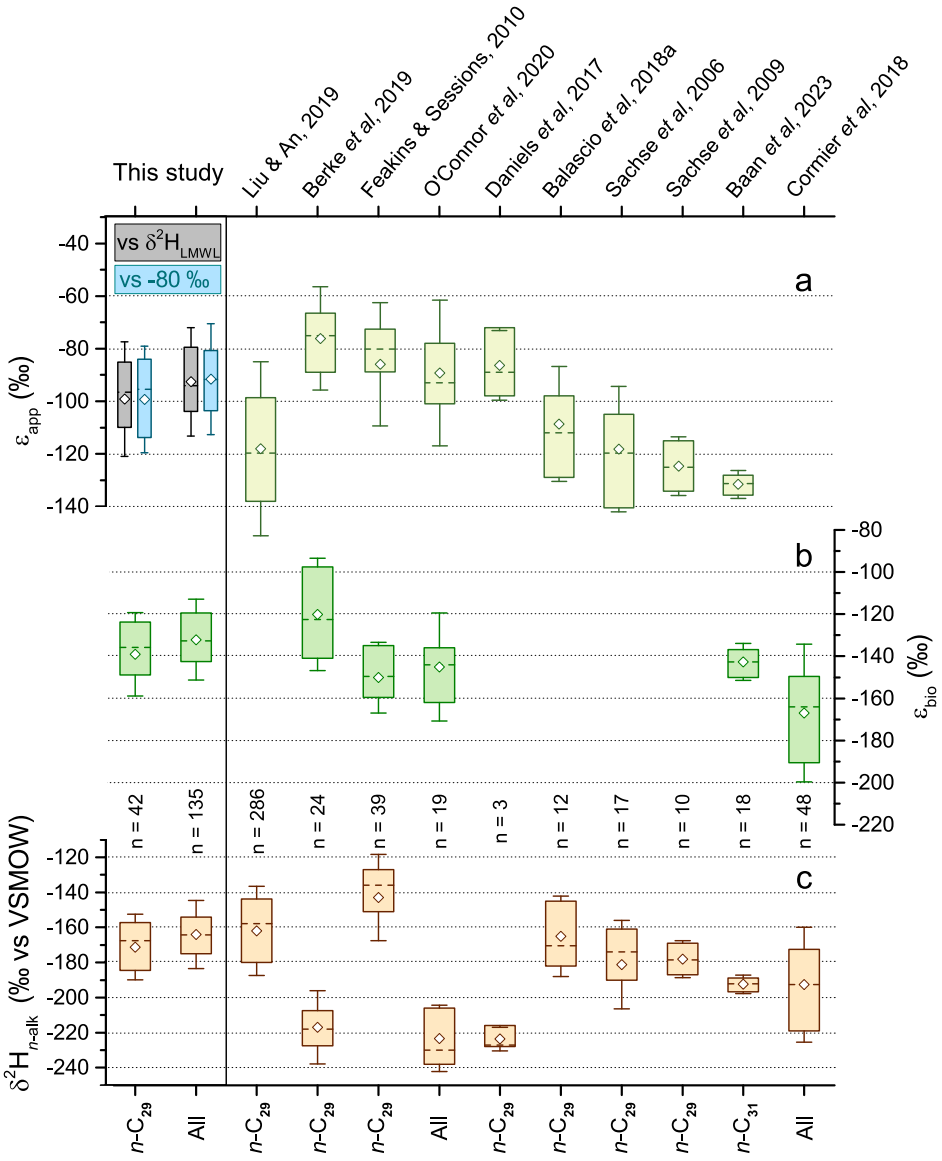

Fig. 8. Apparent fractionation (ε_{app}; a), biosynthetic fractionation (ε_{bio}; b) and δ^2H_{n-alk} (c) comparison between studies reporting natural vegetation isotope analyses results. We present only the wild type data which does not include any lab-grown plants. The ε_{app} values reported in this study (from dicots) are calculated between δ^2H_{n-alk} value and the mean source water δ^2H_{LMWL} (black boxes); we also calculated the ε_{app} between δ^2H_{n-alk} and the mean annual δ^2H_{precip} (–80 ‰; blue boxes). Top axis shows the data source from other studies (Sachse et al., 2006, 2009; Feakins and Sessions, 2010; Daniels et al., 2017; Balascio et al., 2018a; Cormier et al., 2018; Berke et al., 2019; northern mid and high–latitude data by Liu and An, 2019; O'Connor et al., 2020; Baan et al., 2023). The studies by Liu and An (2019), Daniels et al (2017), Balascio et al (2018a) and Cormier et al (2018) include some grasses. The δ^2H_{n-alk} and fractionation factors reported by Berke et al (2019), Feakins and Sessions (2010), O'Connor et al (2020), Sachse et al (2006, 2009) and Baan et al (2023) do not include grasses. The n values represent the total number of δ^2H_{n-alk}, ε_{app} and/or ε_{bio}. Bottom axis shows the n–alkanes used to calculate the reported values where "all" indicates that every chain length δ^2H value measured was incorporated. The combined ("all") values in our study are non-weighted. Boxes represent interquartile range, middle dashed lines are median values, diamonds are mean values and the whiskers mark the 1σ range. (For interpretation of the references to colour in this figure legend, the reader is referred to the web version of this article.)

interpretations which suggest that grasses may be comparatively underrepresented in the δ^2H_{n-alk} pool compared to trees (Diefendorf and Freimuth, 2017). It is also possible that in some cases the sedimentary δ^2H_{n-alk} might vary in response to large plant stresses that cause changes in the ε_{bio}, even when δ^2H_{precip} values remain constant (Kahmen et al., 2013b). Nonetheless, the δ^2H_{C29} values from our measurements alongside the ε_{bio} can be used to reconstruct δ^2H_{lw} as demonstrated above, given that on balance, ε_{bio} values are likely to remain stable over time. Reconstructing past δ^2H_{precip} values by applying the calculated ε_{app} values to the sedimentary $\delta^2H_{n\text{-}alk}$ proxy is also possible, but carries the additional assumption that the ^2H-enrichment of the leaf water has remained relatively constant through time.

6. Conclusions

In this study we addressed the effects of plant water isotopic fractionation from precipitation to biomarkers of seven plant species in Estonia. The δ^2H values from xylem and leaf water of these seven species in addition to soil water indicate that the plants drew their water from the upper 40 cm soils, which largely reflected the meteoric water signature. Isotopic fractionation from leaf transpiration in local plants was stable and evaporation from soil relatively small. Leaf water isotopic enrichment could be modeled and serves as an important link for estimating fractionation factors for all species individually at both of our study locations. The *n*-alkane content in the leaf biomass reveals that the

biomarker distribution was consistent between the two sites, and out of the studied species, *Alnus incana* and *Vaccinium myrtillus* contributed to the sediments the most. Leaf and surface lake sediment *n*-alkane analysis shows that the distribution and δ^2H_{n-alk} values were relatively consistent between the two catchments and within the sediment, implying that these *n*-alkanes are major sources to the sediments. Our relatively lower ε_{app} suggests that it would be improper to apply the ε_{app} values from lower latitudes to reconstruct past hydroclimatic conditions at our study sites. As such, the fractionation factors specific to the area describing the distinct climate conditions, environmental factors and vegetation specifics are required. In addition, we find that the most abundantly occurring alkane in our tree leaves is the *n*-C_{29}. Our estimated ε_{app} (–99 ± 20 ‰) calculated from the plants is less than the ε_{app} calculated from the sediments (–133 ‰). This suggests either that (1) there was a significant contribution of grass-derived lipids to the lake sediments, (2) the lipids from trees with lower δ^2H values contributed a greater proportion of lipids to the sediment, (3) the ε_{app} values in the year in which we conducted our study differed from those of the long-term mean represented in the past few years of sedimentation, or (4) a combination of these factors occurred. Although the ε_{bio} values tend to vary among sites with the highest difference observed between species, our reported average does fall within previously reported values with no major deviations and a modest overall variability. This implies that the basin-specific isotope fractionation factors that have been determined through this work can improve interpretations of sedimentary records by applying the plant-derived ε_{app} on lacustrine δ^2H_{n-alk} proxies which contain information about the timing and magnitude of past hydrological change (Rach et al., 2017). This research will provide further constraints for sedimentary organic geochemistry and paleoclimate studies in other similar mid- and high-latitude regions. It also furthers our understanding of how species-specific hydrogen isotope fractionations can be applied for more targeted applications of sedimentary plant wax δ^2H values that go beyond the global scale correlations with mean annual precipitation.

Declaration of Competing Interest

The authors declare that they have no known competing financial interests or personal relationships that could have appeared to influence the work reported in this paper.

Data availability

Data will be made available on request.

Acknowledgements

We thank Dr. Dirk Sachse for help with the biomarker method development in the laboratory, and the Eensalu family members for assistance in the field and for building a custom soil corer. We also thank Ansis Blaus for help with plant identification. This work was supported by Erasmus+ World program, Samuel S. Goldich Fund scholarship by the Department of Earth Atmosphere and Environment at Northern Illinois University, Student Research Assistance Grant by the Society for Sedimentary Geology (SEPM), Tilford Fund scholarship by the Association of Environmental and Engineering Geologists (AEG) Foundation and a Tamkivi Foundation scholarship for Natural Sciences by the Estonian National Culture Foundation awarded to ME. This project was also funded by the U.S. National Science Foundation, International Research Experiences for Students (IRES) grant (OISE-1827135). We thank one anonymous reviewer as well as Dr. Josef P. Werne for helpful feedback, and Dr. Elizabeth Minor for editorial handling of this manuscript.

Appendix A. Supplementary material

Supplementary data to this article can be found online at https://doi.org/10.1016/j.orggeochem.2023.104674.

References

Ahas, R. (Ed.), 2001. Eesti Looduse Kalender (Estonian Nature Calendar), 90. Tartu Ülikool, Geograafia Instituut.
Amin, A., Zuecco, G., Geris, J., Schwendenmann, L., McDonnell, J.J., Borga, M., Penna, D., 2020. Depth distribution of soil water sourced by plants at the global scale: A new direct inference approach. Ecohydrology 13, e2177.
Baan, J., Holloway-Phillips, M., Nelson, D.B., Kahmen, A., 2023. The metabolic sensitivity of hydrogen isotope fractionation differs between plant compounds. Phytochemistry 207, 113563.
Balascio, N.L., D'Andrea, W.J., Anderson, R.S., Wickler, S., 2018a. Influence of vegetation type on n-alkane composition and hydrogen isotope values from a high latitude ombrotrophic bog. Organic Geochemistry 121, 48–57.
Balascio, N.L., D'Andrea, W.J., Gjerde, M., Bakke, J., 2018b. Hydroclimate variability of High Arctic Svalbard during the Holocene inferred from hydrogen isotopes of leaf waxes. Quaternary Science Reviews 183, 177–187.
Barnard, R.L., De Bello, F., Gilgen, A.K., Buchmann, N., 2006. The δ18O of root crown water best reflects source water δ18O in different types of herbaceous species. Rapid Communications in Mass Spectrometry 20, 3799–3802.
Basler, D., 2016. Evaluating phenological models for the prediction of leaf-out dates in six temperate tree species across central Europe. Agricultural and Forest Meteorology 217, 10–21.
Berke, M.A., Cartagena Sierra, A., Bush, R., Cheah, D., O'Connor, K., 2019. Controls on leaf wax fractionation and δ2H values in tundra vascular plants from western Greenland. Geochimica et Cosmochimica Acta 244, 565–583.
Bray, E.E., Evans, E.D., 1961. Distribution of n-paraffins as a clue to recognition of source beds. Geochimica et Cosmochimica Acta 22, 2–15.
Brinkmann, N., Seeger, S., Weiler, M., Buchmann, N., Eugster, W., Kahmen, A., 2018. Employing stable isotopes to determine the residence times of soil water and the temporal origin of water taken up by Fagus sylvatica and Picea abies in a temperate forest. New Phytologist 219, 1300–1313.
Buck, A.L., 1981. New equations for computing vapour pressure and enhancement factor. Journal of Applied Meteorology 20, 1527–1532.
Bush, R.T., McInerney, F.A., 2013. Leaf wax n-alkane distributions in and across modern plants: Implications for paleoecology and chemotaxonomy. Geochimica et Cosmochimica Acta 117, 161–179.
Carlson, R.E., 1977. A trophic state index for lakes 1. Limnology and Oceanography 22, 361–369.
Cernusak, L.A., Barbour, M.M., Arndt, S.K., Cheesman, A.W., English, N.B., Feild, T.S., Helliker, B.R., Holloway-Phillips, M.M., Holtum, J.A., Kahmen, A., McInerney, F.A., 2016. Stable isotopes in leaf water of terrestrial plants. Plant, Cell & Environment 39, 1087–1102.
Chen, Y., Helliker, B.R., Tang, X., Li, F., Zhou, Y., Song, X., 2020. Stem water cryogenic extraction biases estimation in deuterium isotope composition of plant source water. Proceedings of the National Academy of Sciences of the United States of America 117, 33345–33350.
Clifton-Brown, J.C., Jones, M.B., 1999. Alteration of transpiration rate, by changing air vapour pressure deficit, influences leaf extension rate transiently in Miscanthus. Journal of Experimental Botany 50, 1393–1401.
Coplen, T.B., 2011. Guidelines and recommended terms for expression of stable-isotope-ratio and gas-ratio measurement results. Rapid Communications in Mass Spectrometry 25, 2538–2560.
Cormier, M.A., Werner, R.A., Sauer, P.E., Gröcke, D.R., Leuenberger, M.C., Wieloch, T., Schleucher, J., Kahmen, A., 2018. 2H-fractionations during the biosynthesis of carbohydrates and lipids imprint a metabolic signal on the δ2H values of plant organic compounds. New Phytologist 218, 479–491.
Craig, H., Gordon, L., 1965. Deuterium and oxygen 18 variations in the ocean and the marine atmosphere. In: Tongiorgi, E. (Ed.), Stable Isotopes in Oceanographic Studies and Paleotemperatures. Consiglio Nazionale delle Ricerche, Laboratorio di Geologia Nucleare, Pisa, pp. 277–374.
Daniels, W.C., Russell, J.M., Giblin, A.E., Welker, J.M., Klein, E.S., Huang, Y., 2017. Hydrogen isotope fractionation in leaf waxes in the Alaskan Arctic tundra. Geochimica et Cosmochimica Acta 213, 216–236.
Diefendorf, A.F., Freeman, K.H., Wing, S.L., Graham, H.V., 2011. Production of n-alkyl lipids in living plants and implications for the geologic past. Geochimica et Cosmochimica Acta 75, 7472–7485.
Diefendorf, A.F., Freimuth, E.J., 2017. Extracting the most from terrestrial plant-derived n-alkyl lipids and their carbon isotopes from the sedimentary record: A review. Organic Geochemistry 103, 1–21.
Farquhar, G.D., Cernusak, L.A., Barnes, B., 2007. Heavy water fractionation during transpiration. Plant physiology 143, 11–18.
Farquhar, G.D., Lloyd, J., 1993. Carbon and oxygen isotope effects in the exchange of carbon dioxide between terrestrial plants and the atmosphere. In: Ehleringer, J.R., Hall, A.E., Farquhar, G.D. (Eds.), Stable Isotopes and Plant Carbon-Water Relations. Academic Press, San Diego, CA, USA, pp. 47–70.
Feakins, S.J., 2013. Pollen-corrected leaf wax D/H reconstructions of northeast African hydrological changes during the late Miocene. Palaeogeography, Palaeoclimatology, Palaeoecology 374, 62–71.

Feakins, S.J., Sessions, A.L., 2010. Controls on the D/H ratios of plant leaf waxes in an arid ecosystem. Geochimica et Cosmochimica Acta 74, 2128–2141.
Flanagan, L.B., Orchard, T.E., Tremel, T.N., Rood, S.B., 2019. Using stable isotopes to quantify water sources for trees and shrubs in a riparian cottonwood ecosystem in flood and drought years. Hydrological Processes 33, 3070–3083.
Freimuth, E.J., Diefendorf, A.F., Lowell, T.V., Wiles, G.C., 2019. Sedimentary n-alkanes and n-alkanoic acids in a temperate bog are biased toward woody plants. Organic Geochemistry 128, 94–107.
Herrera-Herrera, A.V., Leierer, L., Jambrina-Enríquez, M., Connolly, R., Mallol, C., 2020. Evaluating different methods for calculating the Carbon Preference Index (CPI): Implications for palaeoecological and archaeological research. Organic Geochemistry 146, 104056.
IAEA. International Atomic Energy Agency/World Meteorological OrganizationGlobal Network of Isotopes in Precipitation. The GNIP Database. https://nucleus.iaea.org/wiser.
Jouzel, J., Merlivat, L., 1984. Deuterium and oxygen 18 in precipitation: Modeling of the isotopic effects during snow formation. Journal of Geophysical Research: Atmospheres 89 (D7), 11749–11757.
Kahmen, A., Hoffmann, B., Schefuß, E., Arndt, S.K., Cernusak, L.A., West, J.B., Sachse, D., 2013a. Leaf water deuterium enrichment shapes leaf wax n-alkane δD values of angiosperm plants II: Observational evidence and global implications. Geochimica et Cosmochimica Acta 111, 50–63.
Kahmen, A., Schefuß, E., Sachse, D., 2013b. Leaf water deuterium enrichment shapes leaf wax n-alkane δd values of angiosperm plants I: Experimental evidence and mechanistic insights. Geochimica et Cosmochimica Acta 111, 39–49.
Kalm, V., 2006. Pleistocene chronostratigraphy in Estonia, southeastern sector of the Scandinavian glaciation. Quaternary Science Reviews 25, 960–975.
Keskkonnaagentuur, 2022. Estonian Nature Information System (EELIS). https://infoleht.keskkonnainfo.ee/ (accessed 5.27.22).
Klein, E.S., Nolan, M., McConnell, J., Sigl, M., Cherry, J., Young, J., Welker, J.M., 2016. McCall Glacier record of Arctic climate change: Interpreting a northern Alaska ice core with regional water isotopes. Quaternary Science Reviews 131, 274–284.
Konecky, B., Dee, S.G., Noone, D.C., 2019. WaxPSM: A Forward Model of Leaf Wax Hydrogen Isotope Ratios to Bridge Proxy and Model Estimates of Past Climate. Journal of Geophysical Research: Biogeosciences 124, 2107–2125.
Krupková, L., Marková, I., Havránková, K., Pokorný, R., Urban, O., Šigut, L., Pavelka, M., Cienciala, E., Marek, M.V., 2017. Comparison of different approaches of radiation use efficiency of biomass formation estimation in Mountain Norway spruce. Trees - Structure and Function 31, 325–337.
Ladd, S.N., Maloney, A.E., Nelson, D.B., Prebble, M., Camperio, G., Sear, D.A., Hassall, J. D., Langdon, P.G., Sachs, J.P., Dubois, N., 2021. Leaf wax hydrogen isotopes as a hydroclimate proxy in the tropical Pacific. Journal of Geophysical Research: Biogeosciences 126 e2020JG005891.
Landwehr, J.M., Coplen, T.B., 2006. Line-conditioned excess: a new method for characterizing stable hydrogen and oxygen isotope ratios in hydrologic systems. International Conference on Isotopes in Environmental Studies 132–135.
Lauteri, M., Alessio, G.A., Paris, P., 2006. Using oxygen stable isotopes to investigate the soil-plant-atmosphere hydraulic continuum in complex stands of walnut. Acta Horticulturae 705, 223–230.
Liu, J., An, Z., 2019. Variations in hydrogen isotopic fractionation in higher plants and sediments across different latitudes: Implications for paleohydrological reconstruction. Science of the Total Environment 650, 470–478.
Liu, J., Liu, W., An, Z., Yang, H., 2016. Different hydrogen isotope fractionations during lipid formation in higher plants: Implications for paleohydrology reconstruction at a global scale. Scientific Reports 6, 19711.
Maffei, M., 1996. Chemotaxonomic significance of leaf wax alkanes in the gramineae. Biochemical Systematics and Ecology 24, 53–64.
McCutcheon, R.J., McNamara, J.P., Kohn, M.J., Evans, S.L., 2017. An evaluation of the ecohydrological separation hypothesis in a semiarid catchment. Hydrological Processes 31, 783–799.
McFarlin, J.M., Axford, Y., Masterson, A.L., Osburn, M.R., 2019. Calibration of modern sedimentary δ2H plant wax-water relationships in Greenland lakes. Quaternary Science Reviews 225, 105978.
McInerney, F.A., Helliker, B.R., Freeman, K.H., 2011. Hydrogen isotope ratios of leaf wax n-alkanes in grasses are insensitive to transpiration. Geochimica et Cosmochimica Acta 75, 541–554.
Nelson, D.B., Ladd, S.N., Schubert, C.J., Kahmen, A., 2018. Rapid atmospheric transport and large-scale deposition of recently synthesized plant waxes. Geochimica et Cosmochimica Acta 222, 599–617.
Nelson, D.B., Basler, D., Kahmen, A., 2021. Precipitation isotope time series predictions from machine learning applied in Europe. Proceedings of the National Academy of Sciences 118 e2024107118.
Newberry, S.L., Kahmen, A., Dennis, P., Grant, A., 2015. n-Alkane biosynthetic hydrogen isotope fractionation is not constant throughout the growing season in the riparian tree Salix viminalis. Geochimica et Cosmochimica Acta 165, 75–85.
Newberry, S.L., Nelson, D.B., Kahmen, A., 2017. Cryogenic vacuum artifacts do not affect plant water-uptake studies using stable isotope analysis. Ecohydrology 10, e1892.
O'Connor, K.F., Berke, M.A., Ziolkowski, L.A., 2020. Hydrogen isotope fractionation in modern plants along a boreal-tundra transect in Alaska. Organic Geochemistry 147, 104064.
Palusalu, M., Poska, A., Väli, V., Vassiljev, J., Stansell, N., Eensalu, M., 2023. In: Järvet, A. (Ed.), Yearbook of the Estonian Geographical Society, 46, pp. 23–63.
Putman, A.L., Fiorella, R.P., Bowen, G.J., Cai, Z., 2019. A Global Perspective on Local Meteoric Water Lines: Meta-analytic Insight Into Fundamental Controls and Practical Constraints. Water Resources Research 55, 6896–6910.
Rach, O., Brauer, A., Wilkes, H., Sachse, D., 2014. Delayed hydrological response to Greenland cooling at the onset of the Younger Dryas in western Europe. Nature Geoscience 7, 109–112.
Rach, O., Kahmen, A., Brauer, A., Sachse, D., 2017. A dual-biomarker approach for quantification of changes in relative humidity from sedimentary lipid D/H ratios. Climate of the Past 13, 741–757.
Rodionov, S.N., 2004. A sequential algorithm for testing climate regime shifts. Geophysical Research Letters 31, 2–5.
Sachse, D., Radke, J., Gleixner, G., 2004. Hydrogen isotope ratios of recent lacustrine sedimentary n-alkanes record modern climate variability. Geochimica et Cosmochimica Acta 68, 4877–4889.
Sachse, D., Radke, J., Gleixner, G., 2006. δD values of individual n-alkanes from terrestrial plants along a climatic gradient - Implications for the sedimentary biomarker record. Organic Geochemistry 37, 469–483.
Sachse, D., Kahmen, A., Gleixner, G., 2009. Significant seasonal variation in the hydrogen isotopic composition of leaf-wax lipids for two deciduous tree ecosystems (Fagus sylvativa and Acer pseudoplatanus). Organic Geochemistry 40, 732–742.
Sachse, D., Gleixner, G., Wilkes, H., Kahmen, A., 2010. Leaf wax n-alkane δD values of field-grown barley reflect leaf water δD values at the time of leaf formation. Geochimica et Cosmochimica Acta 74, 6741–6750.
Sachse, D., Billault, I., Bowen, G.J., Chikaraishi, Y., Dawson, T.E., Feakins, S.J., Freeman, K.H., Magill, C.R., McInerney, F.A., Van Der Meer, M.T.J., Polissar, P., Robins, R.J., Sachs, J.P., Schmidt, H.L., Sessions, A.L., White, J.W.C., West, J.B., Kahmen, A., 2012. Molecular paleohydrology: Interpreting the hydrogen-isotopic composition of lipid biomarkers from photosynthesizing organisms. Annual Review of Earth and Planetary Sciences 40, 221–249.
Schimmelmann, A., Lewan, M.D., Wintsch, R.P., 1999. D/H isotope ratios of kerogen, bitumen, oil, and water in hydrous pyrolysis of source rocks containing kerogen types I, II, IIS, and III. Geochimica et Cosmochimica Acta 63, 3751–3766.
Shuman, B., Huang, Y., Newby, P., Wang, Y., 2006. Compound-specific isotopic analyses track changes in seasonal precipitation regimes in the Northeastern United States at ca 8200 cal yr BP. Quaternary Science Reviews 25, 2992–3002.
Smith, F.A., Freeman, K.H., 2006. Influence of physiology and climate on δD of leaf wax n-alkanes from C3 and C4 grasses. Geochimica et Cosmochimica Acta 70, 1172–1187.
Song, X., Barbour, M.M., Farquhar, G.D., Vann, D.R., Helliker, B.R., 2013. Transpiration rate relates to within- and across-species variations in effective path length in a leaf water model of oxygen isotope enrichment. Plant, Cell and Environment 36, 1338–1351.
Sprenger, M., Tetzlaff, D., Buttle, J., Carey, S.K., McNamara, J.P., Laudon, H., Shatilla, N. J., Soulsby, C., 2018. Storage, mixing, and fluxes of water in the critical zone across northern environments inferred by stable isotopes of soil water. Hydrological Processes 32, 1720–1737.
Stansell, N.D., Klein, E.S., Finkenbinder, M.S., Fortney, C.S., Dodd, J.P., Terasmaa, J., Nelson, D.B., 2017. A stable isotope record of Holocene precipitation dynamics in the Baltic region from Lake Nuudsaku, Estonia. Quaternary Science Reviews 175, 73–84.
Tipple, B.J., Berke, M.A., Doman, C.E., Khachaturyan, S., Ehleringer, J.R., 2013. Leaf-wax n-alkanes record the plant-water environment at leaf flush. Proceedings of the National Academy of Sciences of the United States of America 110, 2659–2664.
Tooming, H., 1996. Changes in surface albedo and air temperature at Tartu, Estonia. Tellus, Series A: Dynamic Meteorology and Oceanography 48, 722–726.
van den Bos, V., Engels, S., Bohncke, S.J.P., Cerli, C., Jansen, B., Kalbitz, K., Peterse, F., Renssen, H., Sachse, D., 2018. Late Holocene changes in vegetation and atmospheric circulation at Lake Uddelermeer (The Netherlands) reconstructed using lipid biomarkers and compound-specific δD analysis. Journal of Quaternary Science 33, 100–111.
Vargas, A.I., Schaffer, B., Yuhong, L., da Sternberg, L., S.l.,, 2017. Testing plant use of mobile vs immobile soil water sources using stable isotope experiments. New Phytologist 215, 582–594.
Wesołowski, T., Rowiński, P., 2006. Timing of bud burst and tree-leaf development in a multispecies temperate forest. Forest Ecology and Management 237, 387–393.
West, J.B., Sobek, A., Ehleringer, J.R., 2008. A simplified GIS approach to modeling global leaf water isoscapes. PLoS one 3, e2447.
Yang, H., Liu, W., Leng, Q., Hren, M.T., Pagani, M., 2011. Variation in n-alkane δD values from terrestrial plants at high latitude: Implications for paleoclimate reconstruction. Organic Geochemistry 42, 283–288.
Zech, M., Pedentchouk, N., Buggle, B., Leiber, K., Kalbitz, K., Marković, S.B., Glaser, B., 2011. Effect of leaf litter degradation and seasonality on D/H isotope ratios of n-alkane biomarkers. Geochimica et Cosmochimica Acta 75, 4917–4928.